A Review on Recent Advancements of Biomedical Radar for Clinical Applications

Shuqin Dong, *Student Member, IEEE*, Li Wen, *Student Member, IEEE*, Yangtao Ye, *Student Member, IEEE*, Zhi Zhang, Yi Wang, Zhiwei Liu, Qing Cao, Yuchen Xu, Changzhi Li, *Fellow, IEEE*, and Changzhan Gu, *Senior Member, IEEE*

***Abstract*—The field of biomedical radar has witnessed significant advancements in recent years, paving the way for innovative and transformative applications in clinical settings. Most medical instruments invented to measure human activities rely on contact electrodes, causing discomfort. Thanks to its non-invasive nature, biomedical radar is particularly valuable for clinical applications. A significant portion of the review discusses improvements in radar hardware, with a focus on miniaturization, increased resolution, and enhanced sensitivity. Then, this paper also delves into the signal processing and machine learning techniques tailored for radar data. This review will explore the recent breakthroughs and applications of biomedical radar technology, shedding light on its transformative potential in shaping the future of clinical diagnostics, patient and elderly care, and healthcare innovation.**

***Index Terms*—Biomedical radar, clinical application, cardiopulmonary activity, displacement detection, medical Internet of Things.**

***Impact Statement*— This review serves as a testament to the transformative impact of radar systems on clinical applications, emphasizing their potential to enhance diagnostics, optimize patient care, and contribute to the ongoing evolution of healthcare practices.**

Manuscript received 29 January 2024; revised 10 March 2024 and 7 May 2024; accepted 7 May 2024. Date of publication 15 May 2024; date of current version 15 August 2024. This work was supported in part by the National Science Foundation of China under Grant 62188102 and Grant 62171277, in part by Shanghai Jiao Tong University Medical-Engineering Interdisciplinary Research Fund under Grant YG2023QNA30, and in part by Shanghai Municipal Science and Technology Major Project under Grant 2021SHZDZX0102. The review of this article was arranged by Editor Bjoern Michael Eskofier. *(Shuqin Dong and Li Wen contributed equally to this work.) (Corresponding author: Changzhan Gu.)*

Shuqin Dong, Li Wen, Yangtao Ye, and Changzhan Gu are with the State Key Laboratory of Radio Frequency Heterogeneous Integration and MoE Key Laboratory of Artificial Intelligence, Shanghai Jiao Tong University, Shanghai 200240, China, and also with the Hecaray Technology Company Ltd., Shanghai 200240, China (e-mail: changzhan@sjtu.edu.cn).

Zhi Zhang is with the Shanghai General Hospital, Shanghai Jiao Tong University School of Medicine, Shanghai 200080, China.

Yi Wang and Zhiwei Liu are with the International Peace Maternity and Child Health Hospital, Shanghai Jiao Tong University School of Medicine, Shanghai 200030, China.

Qing Cao and Yuchen Xu are with the Ruijin Hospital, Shanghai Jiao Tong University School of Medicine, Shanghai 200025, China.

Changzhi Li is with the Department of Electrical and Computer Engineering, Texas Tech University, Lubbock, TX 79409 USA.

Digital Object Identifier 10.1109/OJEMB.2024.3401105

I. Introduction

BIOMEDICAL radar, a cutting-edge technology at the intersection of radar systems and medical science, has emerged as a powerful tool with diverse clinical applications. By harnessing electromagnetic waves to non-invasively probe and monitor biological phenomena, biomedical radar opens new frontiers in diagnostics, patient monitoring, and therapeutic interventions. This innovative approach capitalizes on the ability of radar systems to detect and analyze subtle changes in biological parameters, offering healthcare professionals unprecedented insights into physiological processes. In the paper, we will introduce the principles of biomedical radar and delve into its promising clinical applications that span from early disease detection to personalized patient care. The convergence of radar technology and biomedical research holds tremendous potential to revolutionize the field of medicine. providing advanced patient-centric healthcare solutions that prioritize patient safety, efficiency, and overall well-being.

Over the past decade, significant strides have been made in the development of biomedical radar systems, propelled by advancements in signal processing, machine learning, and sensor technologies. These systems have evolved from traditional radar applications to sophisticated tools capable of extracting intricate physiological information.

In the early phase, emphasis was placed on statistical detection of fundamental physiological parameters. The concept of noncontact detection of vital signs has been successfully demonstrated in this field before 2000 [1], [2], [3], pioneering a series of theoretical and applied studies. This included the detection of respiratory and heartbeat signals in both single and multiple individuals, the detection of buried human subjects in rubble, the localization of human targets, the fusion detection of physiological data from multiple perspectives, the assessment of sleep-disordered breathing, the evaluation of respiratory and heartbeat variations in hemorrhaging human subjects, and the intelligent perception of coarse-to-fine human micro-movements.

In the past few years, the research on physiological information detection and health perception based on bio-radar can be broadly categorized into two phases: the early stage focusing on basic statistical detection of physiological characteristics, and the later stage involving the analysis of respiratory and heartbeat rhythms, fine-grained time-varying feature parameter

detection, and relevant research on the assessment of clinical cardiorespiratory diseases.

Previous research has predominantly focused on obtaining basic statistical indicators such as heart rate and respiratory rate, falling short in capturing the fine-grained temporal evolution characteristics of cardiac micro-movements [4], [5], [6], [7]. Ongoing research in the field of bio-radar cardiac and pulmonary micro-movement detection is gradually deepening [8]. The perceptible information hierarchy is shifting from basic, singular statistical indicators towards a more nuanced analysis of the intricate temporal changes in multidimensional features of cardiac micro-movements. These advancements have initiated preliminary health assessments for both healthy individuals and those with cardiorespiratory conditions [9].

The paper starts with the fundamental theory of biomedical radar for clinical application in Section II. It concludes the various architectures of RF front-end and different baseband demodulation and signal processing methods. Section III addresses regulatory concerns, data security, and the need for clinical application. The specific radar-based clinical applications are concluded in Sections IV, V, and VI. The fine detection of respiratory and cardiovascular activities based on radar systems, as well as the extensive clinical applications of radar imaging technology, has been separately introduced. A conclusion will be drawn in Section VII.

II. Biomedical Radar Detection Principle

The inception of biomedical radar for detecting life characteristics dates back to the previous century. It is a crucial non-contact detection method that involves the detection of various micro-motions induced by human physiological activities, thereby obtaining diverse physiological information. Continuous wave (CW) radar stands out as a preferred technology for vital sign detection due to its non-intrusive nature, allowing for contactless and continuous monitoring of physiological parameters [10]. This versatile approach enables real-time data acquisition in diverse settings, from healthcare to security, with the added benefit of remote sensing and penetration through clothing. In this section, we will elucidate several commonly employed architectural frameworks of CW radar systems in contemporary biomedical applications. Additionally, we will provide a detailed exposition on the precise linear demodulation methods for target displacement under each radar architecture. This constitutes the fundamental basis for non-contact vital sign detection in bio-radar applications.

A. Doppler Radar

As a kind of CW radar, Doppler radar is a promising technology for low-power displacement sensing applications, as shown in Fig. 1 [11]. Doppler radar system uses a direct-conversion, which reduces power consumption compared to other radar systems like frequency-modulated continuous wave (FMCW) radar. Doppler radar using quadrature architecture, eliminates detection nulls. The radar system also benefits from low in-band phase noise, which leads to low noise floors and high range accuracy and sensitivity [12].

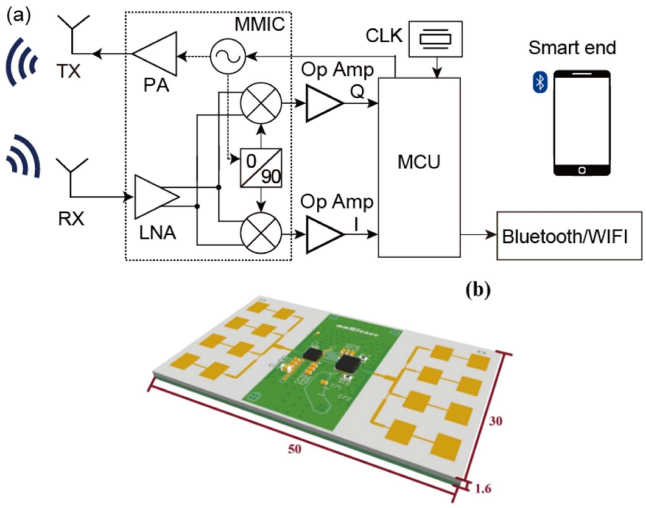

Fig. 1. (a) The block diagram of Doppler radar system. (b) The implementation of designed radar system.

According to the principle of continuous wave Doppler radar, the backscattered electric field $E(t)$ containing the information of target motion $x(t)$ can be expressed as:

$$E(t) = A(t) \cdot \cos[2\pi f_c t + 4\pi x(t)/\lambda + \varphi_0(t)] \quad (1)$$

where $\varphi_0(t)$ includes the phase noise and the phase delay due to the distance between the antenna and target, $A(t)$ is the AC-signal amplitude, f_c is the carrier frequency and λ is the wavelength of the radar carrier.

For the quadrature Doppler radar system, the detected in-phase (I) and quadrature-phase (Q) baseband signals can be described as:

$$I(t) = A_I \cdot \cos[4\pi x(t)/\lambda + \varphi_0 + \Delta\varphi] + DC_I \quad (2)$$

$$Q(t) = A_Q \cdot \sin[4\pi x(t)/\lambda + \varphi_0 + \Delta\varphi] + DC_Q \quad (3)$$

where A_I and A_Q are the amplitudes of the quadrature I/Q signals, respectively, DC_I / DC_Q are the DC offsets, φ_0 is the initial phase of the radar system, and $\Delta\varphi$ is the residual phase noise.

In the previous research, many efforts have been devoted to the accurate reconstruction of the target motion $x(t)$ of the baseband signal. The small angle approximation method is a simple approach for vital sign detection, but it only works when the target movement is negligibly small compared to the wavelength [13]. The arctangent demodulation method can linearly recover the target motion as described in formula (4), but it suffers from a codomain limitation of ($-\pi/2$, $\pi/2$) due to the arctangent transformation and requires supernumerary computation cost for phase unwrapping [14], [15].

$$x(t) = \frac{\lambda}{4\pi}\left\{\arctan\frac{[Q(t) - DC_Q]/A_Q}{[I(t) - DC_I]/A_I} - \varphi_0 - \Delta\varphi\right\} \quad (4)$$

The modified differentiate and cross-multiply (MDACM) algorithm which gets rid of arctangent transformation has been proposed for linear target motion reconstruction with high accuracy and robustness against noise in [16]. It includes two

steps i.e., direct differentiation and cross-multiplication. After the first step, the differentiated *I*/*Q* signals (2)/(3) can be written as follow:

$$\frac{dI(t)}{dt} = -A_I \cdot \sin[4\pi x(t)/\lambda + \varphi_0 + \Delta\varphi] \cdot \frac{4\pi dx(t)}{\lambda dt} \quad (5)$$

$$\frac{dQ(t)}{dt} = A_Q \cdot \cos[4\pi x(t)/\lambda + \varphi_0 + \Delta\varphi] \cdot \frac{4\pi dx(t)}{\lambda dt} \quad (6)$$

After the calibration process, the A_I and A_Q in (5) and (6) can be normalized to 1. Then the cross-multiplied results of (5)–(8) are described as:

$$\frac{dI(t)}{dt} \cdot Q(t) = -\sin^2[4\pi x(t)/\lambda + \varphi_0 + \Delta\varphi] \cdot \frac{4\pi dx(t)}{\lambda dt} \quad (7)$$

$$\frac{dQ(t)}{dt} \cdot I(t) = \cos^2[4\pi x(t)/\lambda + \varphi_0 + \Delta\varphi] \cdot \frac{4\pi dx(t)}{\lambda dt} \quad (8)$$

According to the orthogonality of the trigonometric functions, (7) and (8) can be combined as $I(t) \cdot \mathrm{d}Q(t)/\mathrm{d}t - \mathrm{d}I(t)/\mathrm{d}t \cdot Q(t) = (\sin^2 + \cos^2) \cdot 4\pi\ \mathrm{d}x(t)/\lambda\mathrm{d}t$. After further manipulation, the derivate form of the target motion can be obtained:

$$\frac{dx(t)}{dt} = \frac{\lambda}{4\pi}\left[I(t)\frac{dQ(t)}{dt} - Q(t)\frac{dI(t)}{dt}\right] \quad (9)$$

Obviously, after an integration procedure, the target motion can be linearly reconstructed. Moreover, the integration would suppress the noise brought by differentiators in (9) which also provides anti-noise performance.

For implementation in hardware like digital signal processors (DSPs), the digital-domain MDACM algorithm can be rewritten as:

$$x[n] = \frac{\lambda}{4\pi}\sum_{k=2}^{n} I[k-1]Q[k] - I[k]Q[k-1] \quad (10)$$

B. Low-IF CW Radar

The single-tone CW radar has long been utilized for vital sign detection and many signal processing techniques have been proposed to improve its performance such as DCcal [17], [18], [19], quadrature imbalance correction [20], [21], digital post-distortion (DPoD), MDACM demodulation and so on [22], [23].

Low-IF CW radar addresses issues such as IF carrier leakage and I/Q phase mismatch, which are concerns in conventional Doppler radar. However, low-IF radars still encounter challenges such as high sampling rates for intermediate-frequency signals and wastage of computational resources. Recently, with the asynchronous bandpass sampling technology, low-IF radar allows for very low sampling rates, e.g.,20 Hz, after envelope detection in hardware, reducing the hardware complexity of the radar system.

Fig. 2 shows a block diagram of a coherent low-IF Doppler radar system including an asynchronous bandpass sampling circuitry. Fig. 3 is the implementation of low-IF radar. Regardless of the signal amplitude, the LO signal and IF signal at Tx can be written as

$$s_{LO}(t) = \cos(2\pi\ f_C t + \theta_C) \quad (11)$$

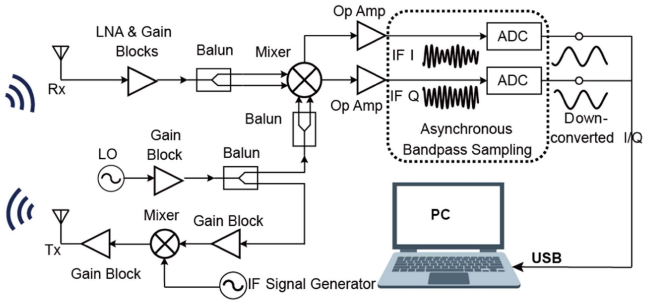

Fig. 2. The block diagram of Low-IF continue wave radar system.

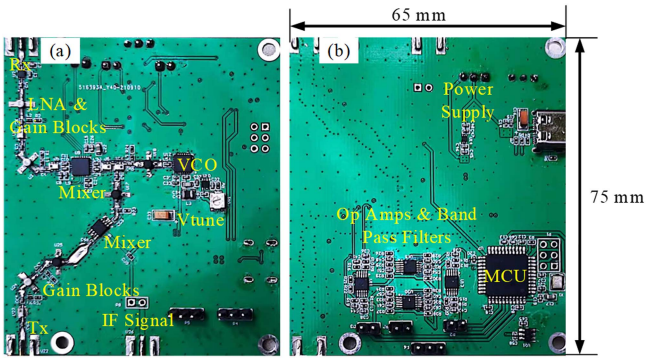

Fig. 3. (a) Top-view and (b) bottom-view photographs of the designed low-IF radar.

$$s_{IF,Tx}(t) = \sin(2\pi\ f_I t + \theta_I), \quad (12)$$

where t is the "fast time", f_C is the LO signal frequency, f_I is the IF signal frequency, and θ_C, θ_I are the initial phases of the RF signal and IF signal, respectively. The LO signal is mixed with the IF signal to obtain the transmitted DSB signal at Tx, which can be written as

$$s_T(t) = \cos(2\pi\ f_C t + \theta_C) \cdot \sin(2\pi\ f_I t + \theta_I). \quad (13)$$

The transmitted signal is reflected by a moving object and other stationary objects in the environment and received by an antenna. After amplification and filtering of the Rx chain, the received signal can be written as

$$s_R(t) = A_1\ s_T(t - t_d) + A_0\ s_T(t - t_s), \quad (14)$$

where $t_d = 2d(\tau)/c$, $t_s = 2d_s/c$, τ is the "slow time", c is the speed of light, $d(\tau) = d_0 + x(\tau)$ is the movement of the target, d_0 is the nominal distance of the target from the radar, $x(\tau)$ is the displacement motion of the target over the "slow time", d_s is the equivalent distance from other stationary objects in the environment to the radar, which is generally considered to be constant, and A_1, A_0 are the amplitudes of the signal carrying displacement information and the unwanted signal respectively. The so-called "fast time" and "slow time" are proposed based on the "stop-and-go" hypothesis [21], which assumes that the target is stationary during each very short period of an IF signal.

After the received signal $s_R(t)$ and the LO signal $s_{LO}(t)$ are mixed by a quadrature mixer and the output signals are low- pass

filtered, the original IF *I*/*Q* signals are obtained, which can be written as

$$S_{IFI}(t) = \mathcal{H}[s_R(t)\cos(2\pi\ f_C\ t + \theta_C)] = A_1\cos[4\pi\ d(\tau)/\lambda]$$
$$\sin\ [2\pi\ f_I(t - t_d) + \theta_I] + A_0\cos(4\pi d_s\ /\lambda)$$
$$\sin[2\pi\ f_I(t - t_s) + \theta_I] \quad (15)$$

$$S_{IFQ}(t) = \mathcal{H}[s_R(t)\sin(2\pi\ f_C\ t + \theta_C)] = A_1\sin[4\pi\ d(\tau)/\lambda]$$
$$\sin[2\pi\ f_I(t - t_d) + \theta_I] + A_0\sin(4\pi d_s\ /\lambda)$$
$$\sin[2\pi\ f_I(t - t_s) + \theta_I], \quad (16)$$

where $\mathcal{H}[\cdot]$ refers to low-pass filtering, $\lambda = c/\ f_c$ is the wavelength of the LO signal. Since d_s is a constant, let $4\pi\ d_s\ /\lambda = \varphi_0$. Moreover, when the low-IF radar performs short-range detection, t_d and t_s are often only a few tens of nanoseconds, while f_I is generally on the order of kHz, so $2\pi\ f_I\ t_d$ and $2\pi\ f_I\ t_s$ can be regarded as zero. Therefore, (5) and (6) can be simplified as

$$s_{IFI}(t) = [A_1\cos\ [4\pi\ d(\tau)/\lambda] + A_0\ \cos(\varphi_0)]\sin(2\pi f_I t + \theta_I) \quad (17)$$

$$s_{IFQ}(t) = [A_1\sin[4\pi\ d(\tau)/\lambda] + A_0\ \sin(\varphi_0)]\sin(2\pi f_I t + \theta_I). \quad (18)$$

According to (7) and (8), it can be seen that the original IF *I*/*Q* signals $s_{IFI}(t)$ and $s_{IFQ}(t)$ are actually sinusoidal signals with frequency f_I, whose envelopes carry the motion information of the target and the DC component caused by the stationary objects. The original IF *I*/*Q* signals are then asynchronous bandpass sampled using two ADCs, as shown in Fig. 1. Then, asynchronous bandpass sampling is leveraged to reduce the sampling rate and ease the demands on digital-to-analog converters. Finally, through the phase demodulation process, the movement of the target $d(\tau)$ can be retrieved without the need for synchronization circuitry or carrier compensation circuitry.

C. FMCW Radar

FMCW radars have ranging capabilities, however, with frequency demodulation alone, the range resolution and accuracy of FMCW radar are the same and directly depend on the radar's frequency modulation bandwidth (f_{BW}). To achieve μm-level movement detection of an object using this method would require an f_{BW} greater than 100 THz, which is currently unfeasible [12]. The method based on phase extraction on a fixed range bin can obtain high-precision displacement information. However, this imposes stringent requirements on the phase consistency and synchronization of sampling with chirp signal for FMCW radar.

In recent years, it has been proven that the LFMCW radar can also measure a subject's displacement motions by tracking the phase history [24], [25]. In [26], [27], the vital signs of multiple people at different radical distances are captured simultaneously with the FMCW radar based on the phase tracking method. In [28], [29], a signal process technique is proposed for vital sign monitoring using FMCW radar, which includes a DC calibration procedure for resolving the DC offset issue caused by the RF leakage.

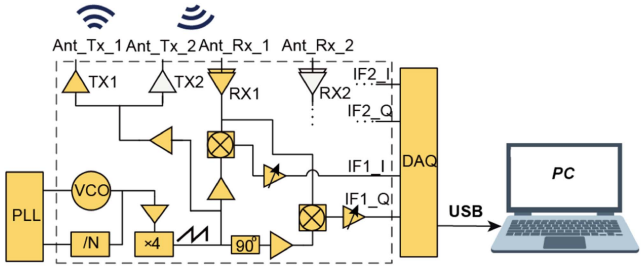

Fig. 4. The block diagram of FMCW radar system.

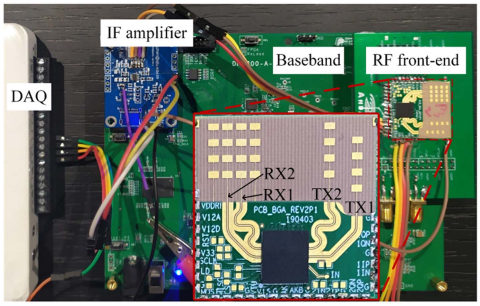

Fig. 5. A picture of the custom-built 79 GHz FMCW radar system. The inset illustrates the mini board that hosts the 2 × 2 CMOS RF front-end chip. [32].

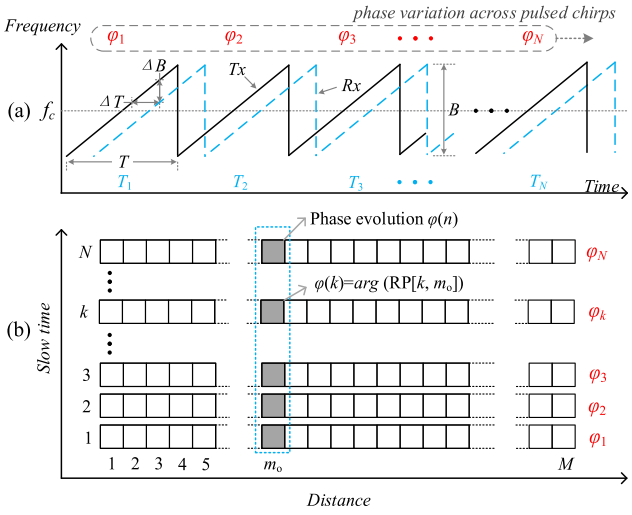

Fig. 6. Extraction of phase history in LFMCW radars: (a) the instantaneous frequency of the Tx and Rx signals. The target's relative displacement motion could be extracted from the phase variation across pulsed chirps; (b) range profiles of sequential beat signals are stacked in rows. The phase variation φ_k could be extracted for each range profile. The greyed column indicates the evolution of phase information at range bin m_o. [32].

Fig. 4 shows the simplified block diagram of the typical single-channel LFMCW radar architectures measuring the vital signs of the subject person. Fig. 5 shows the implantation of the FMCW system. Fig. 6(a) illustrates the instantaneous frequency of the Tx/Rx signals for a typical LFMCW radar, where f_c is the center frequency, T is the interval of the chirp signal, B is the bandwidth, ΔT is the time delay caused by the roundtrip of

the electromagnetic waves, and ΔB is the frequency difference resulting from de-ramping. The transmitted signal within one chirp interval could be mathematically formulated as follows:

$$s_{Tx}(t) = \exp\left[j \cdot (2\pi\ f_c t + \pi\beta\ t^2 + \theta)\right], \tag{19}$$

where t is the so-called "fast time" for the interval [-T/2, T/2], θ is the initial phase, and $\beta = B\ /\ T$ is the chirp rate that presents the steepness of the sawtooth frequency modulation slope. The received signal S_{Rx} is the summation of a number of echoes as the transmitted signals hit the target as well as the surrounding objects. After de-ramping, the output IF beat signal for a single object could be written as:

$$s_b(t\ , \tau) = A \cdot \exp\{j \cdot [(4\pi\beta\ R(\tau)/\ c_0)t + (4\pi\ R(\tau)/\lambda) + \Delta\delta]\ , \tag{20}$$

where A is the amplitude factor considering the path loss and the circuit gain/loss, c_0 is the speed of light, τ is the so-called "slow time", $R(\tau)$ is the absolute distance from the radar to the subject, and $\Delta\delta$ is the residual phase that is negligible in a coherent system [30]. Applying Fourier transform (FFT) on the "fast time" of (2) leads to:

$$s_b(f\ , \tau) = A \cdot T\ \exp[j \cdot (4\pi\ R(\tau)/\lambda)]\mathrm{sinc}(T(f - f_B)), \tag{21}$$

where $f_B = 2\beta\ R(\tau)\ /\ c_0$ is the beat frequency. As shown in Fig. 6(b), the phase-based range-tracking technique selects the range bins m_o where the target sits to reconstruct the phase history representing the displacement of the moving target [32]. The CPRT technique works by combining the phase evolution $\varphi_1,\ \varphi_2, \ldots,\ \varphi_N$ at range bin m_o. Given that f_0 (close to f_B) is the frequency corresponding to the chosen range bin m_o, substituting f_0 into (3) leads to:

$$s_b(f_0\ , \tau) = A \cdot T\ \exp\left[j \cdot (4\pi\ R(\tau)/\lambda)\right]\mathrm{sinc}(T(f_0 - f_B)). \tag{22}$$

(4) can be rewritten as:

$$s_b(\tau) = A'\ \exp\left[j \cdot (4\pi\ R(\tau)/\lambda)\right], \tag{23}$$

where $A' = A \cdot T\ sinc(f_0 - f_B)$ is an amplitude factor with constant phase. As shown in (5), $s_b(\tau)$ is in the same form as the IF signal in the quadrature single-tone CW radar whose working frequency is $f_c = c_0\ /\lambda$ [31]. In this way, the IF signals of an LFMCW radar could be transformed to those of a single-tone CW radar, with the slow time τ being the time-variant parameter. The equivalent quadrature *I*/*Q* signals $S_I(\tau)\ /S_Q(\tau)$as in a single-tone CW radar could be represented as $S_I(\tau) = real\{s_b(\tau)\}$ and $S_Q(\tau) = imag\{s_b(\tau)\}$.

For a single-channel LFMCW radar, the IF output beat signal $s_{bI}(t\ , \tau)$ is the real part of (2). Applying FFT on the "fast time" of $s_{bI}(t\ , \tau)$ leads to:

$$\begin{aligned} s_{bI}(t\ , \tau) = A \cdot (T\ /\ 2)[&\exp\left(j \cdot \varphi(\tau)\right)\mathrm{sinc}(T(f - f_B)) \\ &+ \exp\left(j \cdot -\varphi(\tau)\right)\mathrm{sinc}(T(f + f_B))], \end{aligned} \tag{24}$$

where $\varphi(\tau) = 4\pi\ R(\tau)\ /\lambda$. As f_0 is close to f_B and the sinc function $\sin(\pi x)/\pi x$ decreases fast as x deviates from $x = 0$, $sinc(T(f + f_B)) \approx 0$. Thus, substituting $f\ = f_0$ in (6) results in:

$$s_{bI}(f_0\ , \tau) = (A'\ /\ 2)\ \exp\left[j \cdot (4\pi\ R(\tau)/\lambda)\right], \tag{25}$$

which is in the same form as (5). Therefore, the equivalent *I*/*Q* signals as in a single-tone CW radar can also be synthesized from a single-channel LFMCW radar except that the signal amplitude is reduced by half, which is as expected owing to the merits of the quadrature architecture [32].

III. System Design in Hospital

When introducing biomedical radar into clinical applications, careful consideration should be given to ethical and privacy protection, ensuring the respect of patient rights. The accuracy and reliability of the system must undergo rigorous validation, with a focus on safety to ensure radiation levels comply with standards and the equipment adheres to medical device safety specifications. Consideration of applicability under pathological conditions is essential, along with ensuring the secure transmission and storage of patient data. Training healthcare personnel and establishing standardized operational procedures are imperative to mitigate the risk of misuse. Ensuring system compatibility with other medical devices is crucial to prevent interference. In scenarios involving long-term monitoring and wearability, attention should be directed towards device comfort and durability to facilitate the implementation of prolonged monitoring. A comprehensive consideration of these factors contributes to the effective and safe application of biomedical radar in clinical environments.

A. Ethical Considerations and Electromagnetic Safety

One of the primary ethical concerns associated with the use of radar systems in hospitals is patient privacy. Bio-radar technology, especially when used for patient monitoring, can potentially capture sensitive biological information, such as heart rate, respiratory patterns, or even unique biometric signatures. Clear policies and procedures must be established to ensure that patient data is handled with the utmost confidentiality and in compliance with privacy regulations. Informed consent is another fundamental ethical principle. Researchers must obtain informed consent from patients and hospitals before implementing radar-based monitoring systems. This involves explaining the purpose of technologies, the procedures of experiments, the potential risks of technologies, the data collected, and how it will be used, stored, shared, and destroyed. Meanwhile, transparent communication is essential to build trust between researchers and patients.

Electromagnetic safety is a paramount concern when deploying radar systems in hospital environments. Researchers must adhere to exposure limits and regulations to protect both patients and healthcare workers from potential harm. Regulatory bodies, such as the Federal Communication Commission (FCC) in the United States, provide guidelines on acceptable levels of electromagnetic exposure. Meanwhile, thorough risk assessments should be conducted by hospitals to ensure that radar systems are operating within safe parameters. This includes considering factors such as frequency, power density, and duration of exposure. Regular monitoring and compliance with safety standards are essential to mitigate potential risks. In ICNIRP guidelines

TABLE I
BASIC RESTRICTIONS FOR ELECTROMAGNETIC FIELD EXPOSURE FROM 100 KHZ TO 300 GHZ, FOR AVERAGING INTERVALS $\geq$ 6 MIN [46]

Exposure scenario	Frequency range	Whole-body average SAR (W kg^{-1})	Whole-body average SAR (W kg^{-1})	Whole-body average SAR (W kg^{-1})	Whole-body average SAR (W kg^{-1})
Occupational	100 kHz to 6 GHz	0.4	10	20	NA
	>6 to 300 GHz	0.4	NA	NA	100
General public	100 kHz to 6 GHz	0.08	2	4	NA
	>6 to 300 GHz	0.08	NA	NA	20

TABLE II
BASIC RESTRICTIONS FOR ELECTROMAGNETIC FIELD EXPOSURE FROM 100 KHZ TO 300 GHZ, FOR INTEGRATING INTERVALS $>$ 0 TO $<$ 6 MIN [46]

Exposure scenario	Frequency range	Local Head/Torso SA (kJ kg^{-1})	Whole-body average SAR (W kg^{-1})	Whole-body average SAR (W kg^{-1})
Occupational	100 kHz to 400 MHz	NA	NA	NA
	>400 MHz to 6 GHz	$3.6[0.05+0.95(t/360)^{0.5}$	$7.2[0.025+0.975(t/360)^{0.5}$	NA
	>6 to 300 GHz	NA	NA	$36[0.05+0.95(t/360)^{0.5}$
General public	100 kHz to 400 MHz	NA	NA	NA
	>400 MHz to 6 GHz	$0.72[0.05+0.95(t/360)^{0.5}$	$1.44[0.025+0.975(t/360)^{0.5}$	NA
	>6 to 300 GHz	NA	NA	$7.2[0.05+0.95(t/360)^{0.5}$

TABLE III
BASIC RESTRICTIONS FOR ELECTROMAGNETIC FIELD EXPOSURE FROM 100 KHZ TO 10 MHZ, FOR PEAK SPATIAL VALUES [34]

Exposure scenario	Frequency range	Induced electric field; E_{ind} (V m^{-1})
Occupational	100 kHz to 10 MHz	$2.70 \times 10^{-4} f$
General public	100 kHz to 10 MHz	$1.35 \times 10^{-4} f$

(2020), the limitation of exposure to electromagnetic fields from 100 kHz to 300 GHz is suggested. To be compliant with the basic restrictions, radiofrequency EMF exposure must not exceed the restrictions specified for that EMF frequency in Tables I, II, and III. That is, for any given radiofrequency EMF frequency, relevant whole-body SAR, local SAR, S_ab, SA, U_ab, and induced E-field restrictions must be met simultaneously [34].

Another safety consideration is the potential interference of radar systems with other medical devices. Hospitals are equipped with a wide array of electronic devices. Radar systems must be carefully designed and positioned to prevent interference with critical medical equipment. Before widespread implementation, the electromagnetic compatibility of different electronic devices should be validated.

B. Medical Internet of Things

In the healthcare industry, IoT (Internet of Things) systems are becoming increasingly popular due to their ability to improve patient care. In hospitals, IoMT (Internet of Medical Things) with its set of benefits such as enabling real-time monitoring, providing a more mature and effective solution to collect patient data, and tracking the activities of patients.

Recently, a preliminary radar-based IoT system in the hospital's inpatient area was reported to collect patient daily data, as shown in Fig. 7. The system includes a radar sensor that is placed in the room or on the patient's bed, which collects data on the patient's vital signs and sends it to a central platform or

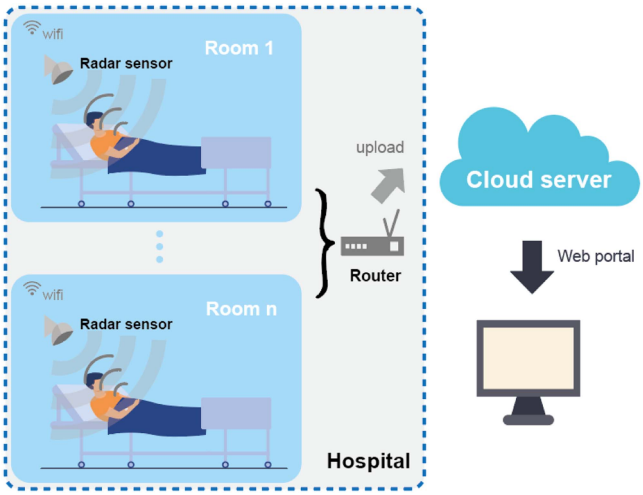

Fig. 7. The potential implementation of the proposed system into hospital care management. [33].

dashboard. The central platform or dashboard can be accessed by healthcare providers, who can use the real-time data to monitor the patient's health status and detect any changes or potential health problems early [33].

Raw radar data is sent to Alibaba Cloud's RDB database 1 through the MQTT queue of the MCU in real time. The algorithm script in the cloud server obtains the newly written record from database 1, and immediately writes it into the specified entry of RDB database 2 after calculating the index. At the same time, it is also sent to the terminal background for visual UI display. The whole system can help healthcare providers take prompt action to prevent complications and improve patient outcomes.

In the system of IoT, the radar sensor consists of a radio frequency (RF) sensing front end, a microcontroller unit (MCU) with embedded baseband signal processing and a wifi module. The pre-processed radar data can be uploaded to the cloud server

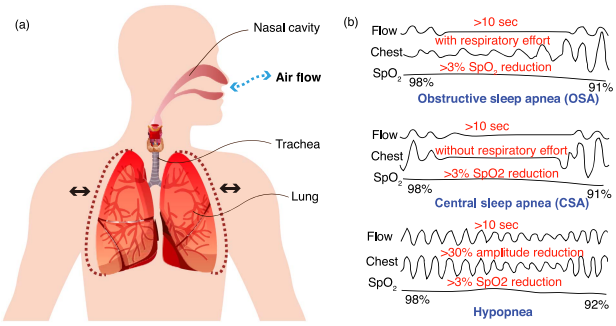

Fig. 8. The diagnostic basis of sleep apnea-hypopnea events based on AASM.

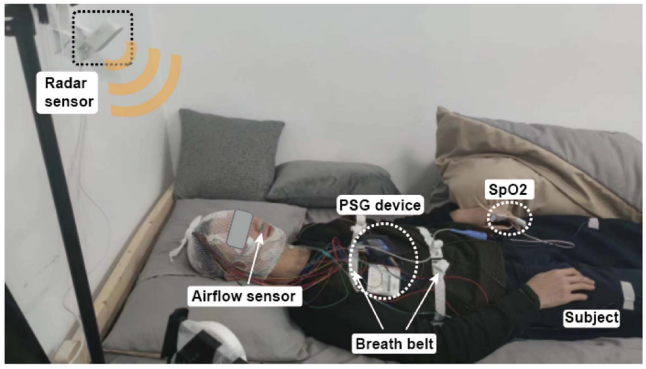

Fig. 9. The experimental setup in sleep lab.

wirelessly through the wifi module. The whole system provides a more mature and effective solution to collect patient data, and tracking the activities of patients than the traditional contact medical system. It should be noted that the wireless transmission module and the RF module operate simultaneously. FreeRTOS is employed in the MCU, with wireless data transmission and RF module control and reception handled as two distinct tasks. Each task has its own operational logic and memory allocation. These tasks are executed based on RTOS system calls, with the higher-priority task being the data sampling task of the RF module. This prioritization is necessary to ensure the stability of the control and sampling frequency of the radar signal.

IV. Clinical Applications Based on Respiration Detection

A. Physiological Model

According to breathing mechanics, during inspiration at rest, the diaphragm contracts and moves inferiorly, which leads to an increase in the longitudinal diameter of the thoracic cavity, while the diameter of the abdominal cavity decreases. In addition, the ribs lift and advance, which causes an increase in the transverse diameter of the thorax. At the same time, contraction of the external intercostal muscles elevates the rib cage (RC) and moves the sternum anteriorly, which also leads to an increase in the transverse and anteroposterior diameter of the thorax [35], as shown in Fig. 8. At rest, exhalation is passive. As the diaphragm relaxes, it moves superiorly and as the external intercostal muscles relax, the RC and sternum return to their resting positions. These actions decrease the size of the thoracic cavity in all dimensions [36].

For radar-based remote sensing scenes, the electromagnetic wave is continuously generated and sent to the target [37], [38], [39]. The reflected echo, containing the human chest movement information, is collected by the receiver.

According to the previous research, there is a linear relationship between the chest-wall movement $x(t)$ and the chest volume change $V(t)$ measured by laser [40]:

$$V(t) \propto x(t). \tag{26}$$

In physiology, the relationship between chest volume change and airflow in humans can be modeled using respiratory physiology principles [41]. One common approach involves using a mathematical model based on the principles of respiratory mechanics:

$$Q(t) = \mathrm{d}V(t) \,/\, dt, \tag{27}$$

where $Q(t)$ represents the airflow as a function of time.

Thus, if the chest-wall movement $x(t)$ can be accurately obtained, the airflow signal can be estimated by formula (27).

Some existing bio-radars reported in the clinical assessment adopted AC architecture, which would introduce the waveform distortion [42]. To accurately track low-frequency relative displacements with minimal distortion, the biomedical radar sensor system needs the DC-coupled radar architecture [42], which lays the foundation for the accurate assessment of the respiratory waveform.

B. Cheyne Stokes Respiration (CSR) Detection

CSR is a phenomenon characterized by regular patterns of gradually increasing and then decreasing tidal volumes. This pattern is often observed in individuals who suffer from severe heart failure (HF) or respiratory drive disorders during sleep. Studies have found that up to 50% of HF patients experience CSR during sleep [43], [44], and some may also have episodes during the day [45], [46]. In both cases, CSR in heart failure patients is associated with a worse prognosis and increased mortality risk [47]. Polysomnography (PSG) is a common diagnostic method in hospitals for evaluating sleep disorders, including CSR identification [46]. Fig. 9 shows the subject wearing the PSG device and lying on the bed in a sleep lab. While PSG provides accurate information with its multiple sensors, it is primarily limited to overnight monitoring in specialized facilities, and wearing PSG can cause discomfort and inconvenience. In contrast, radar-based monitoring methods offer the advantage of long-term monitoring, allowing for non-contact tracking of CSR during daytime and sleep periods. It is more convenient and suitable for continuous respiratory abnormality monitoring.

Shan He et al. (2022) [48] introduced a real-time system that consists of three impulse radio ultrawideband (IR-UWB) radars and a 3D depth camera (Kinect) for robust remote respiratory

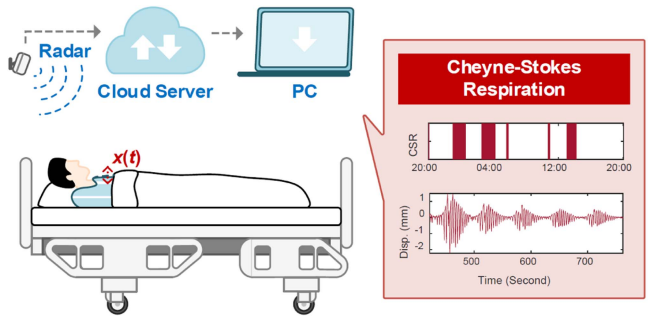

Fig. 10. The schematic diagram illustrating the hospital ward environment's radar-based technique for detecting CSR in respiratory monitoring. [50].

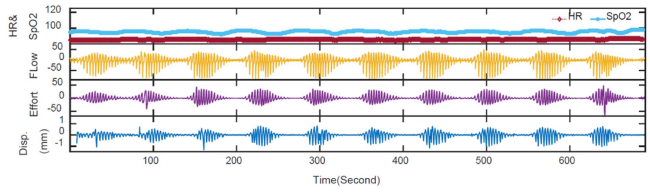

Fig. 11. The signals from multiple PSG sensors and the biomedical radar were compared to identify a 690-second period indicative of CSR during sleep. [50].

rate (RR) estimation and RP classification, including eupnea, CSR, Kussmaul respiration and apnea. The depth camera plays a crucial role in locating individuals in different positions, while the radar signal is utilized for precise recognition of the respiratory pattern once the subject is detected as stationary. Another recent study by Chang Yuan et al. (2022) [49] presented a microwave system to extract CSR RP using two universal software radio peripherals (USRP) based on channel state information (CSI). Although both studies achieved high precision in CSR detection with their classification models, it is important to note that the RP data used in these studies were obtained through simulation with healthy volunteers and have not been tested on real patients. Furthermore, these systems require multiple sensors and can be complex to set up in real monitoring situations. Thus, further validation and optimization are necessary before implementing these systems in clinical practice.

In [50], CSR is first detected on a HF patient with biomedical radar in the ward environment, the scheme diagram of which is shown in Fig. 10. The employed system is CW DC-coupled interferometric radar with DC-tuning function, which is sensitive enough to track the shallow breathing movements of HF patients. Besides, the radar is compact integrating antennas, radio frequency and baseband processing circuit, and it also enables wireless data transmission which is helpful for remote medical care. Clinical experimental results from a two-day monitoring of a HF patient who experienced CSR revealed that the proposed technique could accurately reconstruct the respiratory pattern during both sleep and wakefulness, which also had a good consistency when compared with the PSG results, as shown in Fig. 11. It shows the advantage over the previous work in noncontact wireless CSR monitoring, which may provide insights into long-term tracking of the HF development.

C. Sleep Respiratory Disorder Detection

Sleep apnea-hypopnea syndrome is a prevalent sleep disorder that affects millions of individuals worldwide. Simultaneously with PSG, the radar data of SAS patients were recorded to validate the monitoring feasibility of the sleep apnea-hypopnea events, which consists of obstructive sleep apnea (OSA), central sleep apnea (CSA), and hypopnea. According to these clinical criteria, sleep-apnea events can be classified when the airflow and respiratory efforts amplitude can be accurately measured [51].

As shown in Fig. 9, according to the American Academy of Sleep Medicine (AASM), apnea is defined as the cessation of airflow for at least 10 seconds or longer [52]. Hypopnea is defined as a reduction in the airflow by at least 30% for at least 10 seconds or longer, accompanied by a 4% or greater oxygen desaturation [53]. Based on the accurate respiratory waveform detection, the precise duration of apnea and hypopnea can be calculated, thereby laying the foundation for future apnea-hypopnea events detection.

Some research on radar-based sleep monitoring systems mostly focus on the different respiratory pattern detection [54]. Based on the accurate respiratory waveform reconstruction and machine learning method, obstructive sleep apnea, central sleep apnea, and hypopnea can be automatically identified through radar-based technology [53]. Through comparative analysis with data synchronously collected during overnight sleep experiments alongside multi-channel PSG, and in comparison with sleep breathing disorder events annotated by professional sleep technicians, the accuracy of sleep respiratory disturbance detection based on radar can be validated [55].

D. Infant Respiration Detection

Newborns, especially premature infants, exhibit distinct cardiopulmonary activity patterns due to the immaturity of their respiratory system. Infant respiratory parameters, such as amplitude and rate, differ from those of adults. Their cardiopulmonary activity is weaker and more variable. The RR of infants is typically around 60 bpm, and it is also normal for their heart rate (HR) to exceed 130 bpm. As infants grow older, both their average RR and HR tend to gradually decrease. Periodic breathing (PB), characterized by cycles of breathing and short pauses lasting less than 10 seconds, is a normal occurrence in infants and usually does not require clinical intervention. However, excessive PB has been linked to an increased risk of sudden infant death syndrome (SIDS) [56], [57], [58]. Another respiratory pattern observed in infants is apnea, characterized by longer breathing pauses over 15 or 20 seconds. Apnea episodes can lead to reduced oxygen saturation (SpO2), resulting in hypoxia and a decrease in HR [59]. Studies have shown that apnea occurs in more than half of premature infants and almost all newborns weighing less than 1 kilogram [60]. Untreated recurrent prolonged apnea in infants can lead to adverse long-term effects, such as retinopathy, neurodevelopmental disorders, and an elevated mortality risk [61]. Therefore, it is vital to have close and intelligent monitoring of infant cardiopulmonary activities. However, conventional methods of infant cardiopulmonary

monitoring, such as PSG or electrocardiogram (ECG) alone, may potentially harm the delicate skin of infants.

In a recent study by G. Beltrão et al. [62], a contactless radar-based approach was found to be effective for breathing monitoring in the Neonatal Intensive Care Unit (NICU). The study investigated various scenarios commonly encountered in the NICU's daily routine. Rather than disregarding measurements affected by strong interference, the researchers proposed a novel technique based on time-frequency decomposition to mitigate random body movements. The study involved 12 premature infants, with measurements conducted during noon for three consecutive days, each lasting 25 minutes. The results show an improvement over different scenarios, reducing the overall RMSE to 6.38 bpm. Specifically, measurements in the prone position achieved the best performance, with an RMSE close to 5 bpm. When considering moments without random body movements or reduced interference, the average accuracy of 6 bpm exceeded 80%, with an average RMSE of 4.3 bpm and the best result close to 4 bpm in the prone position.

In [63], a non-contact baby cardiopulmonary monitoring technology based on a K-band continuous wave biomedical radar system is introduced. The biomedical radar system can achieve the detection of micrometer-level displacement and is suitable for non-contact detection of weak cardiopulmonary activity signals in premature infants. In addition, this work also proposes an apnea detection algorithm that can generate adaptive thresholds and personalize the early warning time, which is suitable for infants with irregular breathing rhythms, and can be used in real time for infants with different cardiopulmonary activity states. It also provides more personalized monitoring for premature infants with different gestational age, weight, and disease status. In the experiments, the biomedical radar system is installed at the top of an incubator to keep constant cardiopulmonary monitoring, as shown in Fig. 12(a) and (b). Five premature babies were examined for a total of more than 1, 200 hours. A 35-second result comparison of RR and HR is presented in Fig. 12(c) and (d), showing that the values computed from the respiratory and heartbeat signals are in proximity to the reference values with mean errors below 5 bpm. In 85 episodes lasting 5 to 20 minutes that caused blood oxygen to drop below 90%, the average sensitivity of apnea events per subject detected by the apnea detection algorithm was 0.87, the average correlation coefficient was 0.98, and the average proportion of apnea events less than 10 seconds was found to be 0.42. Fig. 12(e) depicts the apnea detection outcome during an infant PB period, with the longest duration recorded as 10.4 seconds and an average duration of 7.95 seconds.

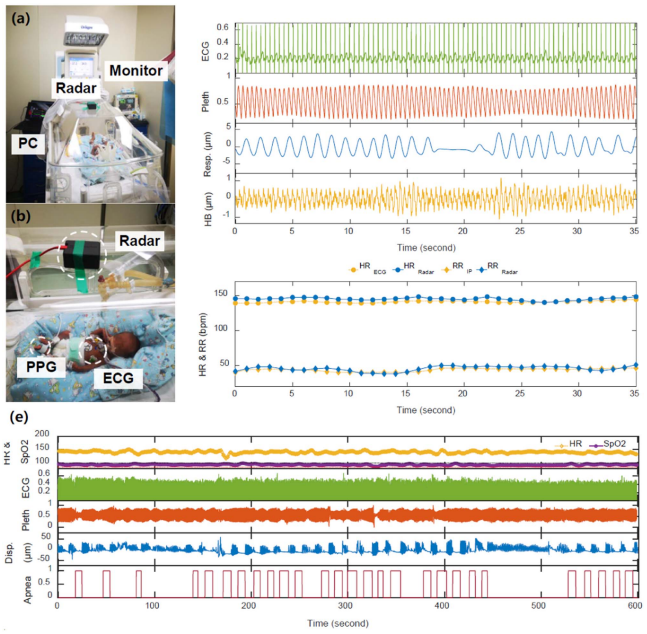

Fig. 12. In the experimental setup (a)-(b), the radar was used to detect cardiorespiratory activity (an example during a 35-second period in (c)-(d)), and the apnea detection algorithm was employed to identify breath pauses (e) [63].

E. Chronic Obstructive Pulmonary Disease (COPD) Detection

COPD is a leading cause of respiratory disease-related deaths, but it is often underdiagnosed, especially in low and middle-income countries [64]. However, the underdiagnosis of COPD remains notably high, partially due to the cost and expertise required for conventional spirometry, which is considered the gold standard for diagnosis. Radar, with its noncontact, low-cost, and high integration characteristics, is being explored as a potential sensor for evaluating pulmonary function in a more accessible way.

Wang et al. (2023) [65] proposed a method that utilizes a 60 GHz FMCW radar system to measure key respiratory indices in spirometry. By capturing the largest one-second chest movements, they represent the relative value of forced expiratory volume in 1 second (FEV1). The study involved 35 participants, including 30 healthy subjects and 5 COPD patients, to measure FEV1, forced vital capacity (FVC), and FEV1/FVC. Experimental results demonstrate an ICC value of 0.8142 for FEV1/FVC between radar-based spirometry and conventional spirometry. The average ICC values for FEV1 and FVC on the validation set are both above 0.75. These findings suggest the potential of radar-based spirometry as an alternative tool for preliminary COPD diagnosis.

S. -T. Tseng et al. [66] developed a radar system with a self-designed CMOS impulse radar chip to extract human respiratory features. The radar chip consists of a digital-to-time converter (DTC), a transmitter, and a receiver. The DTC, based on all-digital standard cells, achieves a timing resolution of 10 ps on a 100-ns time scale, enabling range-gated sensing. To meet data storage needs, the stages of the respiration signal were parameterized using four segments of linear waves. In clinical trials, the wireless sensor system served as a spirometer before and after the 6-minute walk test for respiratory disease identification. Out of 50 participants, 32 had impaired respiratory function. The support vector machine (SVM) based classification accuracy was 73.3%, and for the adaptive network-based fuzzy inference system (ANFIS) analysis, the mean FEV1/FVC

is 75.3, root-mean-square error is 11.35, correlation is 68%, and regression slope is 0.6.

F. Postoperative Monitoring

Changes in RR can serve as an indication of physiological decline and can facilitate early intervention in diseases. However, its usage by clinicians is limited due to the need for continuous RR recording, which requires wearing contact sensors and significant effort for analysis. In a study conducted by K. van Loon et al. (2016) [67], it was discovered that FMCW radar could accurately measure RR in mechanically ventilated patients after surgery. The study involved eight subjects who underwent elective robotic-assisted laparoscopic prostatectomy or hysterectomy. During mechanical ventilation, 796 minutes of data were recorded, while during spontaneous breathing, 521 minutes were recorded. The results of the study revealed that the 95% limits of agreement for RR during mechanical ventilation were −0.12 (−1.76 to 1.51) breaths per minute. Similarly, during spontaneous breathing, the 95% limits of agreement for RR were −0.59 (−5.82 to 4.63) breaths per minute.

V. Clinical Applications Based on Cardiovascular Activity Detection

A. Physiological Model

The human heart is a cone-shaped muscular organ located between the left and right lungs in the middle compartment of a chest. Its function is to pump blood through the atriums and ventricles into the pulmonary or blood circulatory systems, providing oxygen and recycling carbon dioxide to and from the human body [70]. This cardiac motion is rhythmic, synchronous with the bioelectrical "excitations" spontaneously generated in the sinoatrial (SA) node and conducted from the atriums to the ventricles [69]. Heart bioelectrical activity can be detected by electrodes placed at different locations on the skin, and the plotted "action potentials" is known as the ECG [68].

In the past, ballistocardiogram (BCG) and seismocardiogram (SCG) werecommon methods used to measure the mechanical activity of the heart. The BCG measures the body's reaction to the ejection of blood from the heart with each heartbeat. It is based on the principle that when the heart contracts, it ejects blood into the arteries, causing a recoil force that can be detected as subtle movements of the body [71]. SCG involves placing accelerometers or other sensors on the chest to detect the subtle vibrations produced by the heart's mechanical activity. The sensors convert these vibrations into electrical signals, which can then be recorded and analyzed [72].

In the recent work, a physiological model of the heart is demonstrated through the remote measurement of a new type of human mechanical cardiogram called the Doppler cardiogram (DCG) [9]. The DCG is obtained from the Doppler radar, by detecting the combined atrial and ventricular contractions and relaxations conducted to the skin on the human chest. The DCG provides timing information of the P-wave, QRS-waves, and T-wave in ECGs, reflecting the initiation of a bioelectrical impulse at the sinoatrial (SA) node and the activation of the atria, as well as the quick impulse that propagates from the atrioventricular (AV) node down through the Purkinje fibers, causing the ventricles to contract as shown in Fig. 13. The atriums and the ventricles are assumed to be cylinder-like, and the total radial component, denoted as $x(t)$, of the DCG can be estimated as [9]

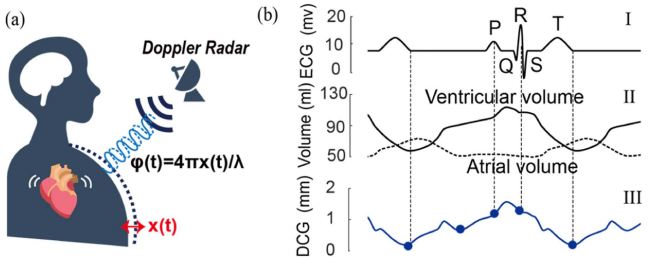

Fig. 13. (a) Scenario of CW Doppler radar vital sign detection, (b) the corresponding among ECG, heart chambers' volume change and DCG which were replicated based on MRI data [85].

$$x(t) \propto \sqrt{V_a(t)} + \sqrt{V_v(t)}. \tag{28}$$

Due to the accurate mechanical activity detection of heart, DCG can reflect the displacement, velocity, and acceleration of the 3-D cardiac motion projected on the skin. This remote sensing technique offers potential applications in personal healthcare, battlefield rescue, and other scenarios.

However, the radar-based heart activity detection of the chest-wall motion x(t) can be modeled as

$$x(t) = xr(t) + D(t), \tag{29}$$

where $x_r(t)$ is the chest-wall motion caused by human breathing.

Obviously, if the respiration motion $x_r(t)$ can be efficiently removed, the heart activity waveform $D(t)$ can be accurately recovered.

B. Cardiogram Detection in Clinical Environment

Fine-grained heart movement detection may help identify subtle abnormalities, track changes in cardiac function over time, and enhance the overall understanding of cardiovascular health. This level of precision can be particularly beneficial in the early detection of cardiac conditions, allowing for timely interventions and ultimately improving patient outcomes. Additionally, in research and clinical trials, fine-grained cardiogram information can contribute to a deeper comprehension of cardiac physiology and aid in the development of advanced diagnostic and therapeutic approaches. To date, commercial cardiogram instruments have been capable of measuring ECG [73], ultrasonic cardiogram (UCG) [74], phonocardiogram (PCG) [75], impedance cardiogram (ICG) [76], ballisto-cardiogram (BCG) [77], and live cardiograms based on magnetic resonance imaging (MRI) [78], [79].

Radar-based high-accuracy movement measurement enables the contactless heart activity detection. In recent publications, some studies are employing the deep learning method, simultaneously collecting radar cardiac cycle and ECG signals to

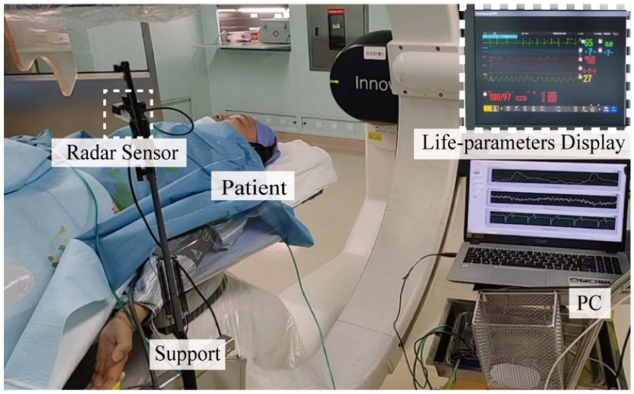

Fig. 14. Experimental setups: DCG measurement experiment in clinical environment. Inset shows the life-parameters monitor display in OT. [85].

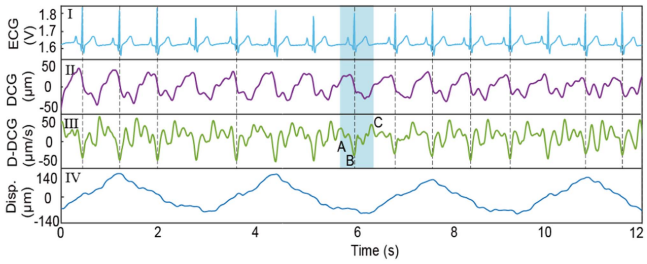

Fig. 15. The simultaneously recorded signals of healthy subject in clinical environment. [85].

reconstruct ECG signals based on radar signals, subsequently obtaining waveforms similar to electrocardiograms [80], [81]. Some studies also employ deep learning methods to obtain seismocardiograms (SCG) from radar signals [82], [83]. There are also related studies utilizing radar technologies to achieve BCG detection [84].

In [85], precise extraction of fine-grained cardiogram waveforms was achieved using a parameterized respiratory filter (PRF) to accurately filter out respiratory motion. Moreover, the clinical experiment was conducted at the bedside in a hybrid operation theatre (OT) of the hospital to verify the performance of the proposed system, as shown in Fig. 14. During the clinical verification, the professional medical device needs to be employed to provide the golden standard, such as simultaneously using patient multi-parameters life monitor as shown in Fig. 14.

Performing differentiation operations on fine-grained cardiac activity waveforms can yield more comprehensive information about heart dynamics. For instance, as extracted in reference [85], the differential DCG (D-DCG) can depict the velocity information of cardiac activity, as illustrated in Fig. 15.

C. Cardiac Timing Detection

Measurement of the rhythmic time intervals of the cardiac cycle offers a quantifiable method to assess cardiac function. Among them, the estimation of heart systolic time intervals (STIs) and R-R interval attracted the most interest due to its clinical value [86].

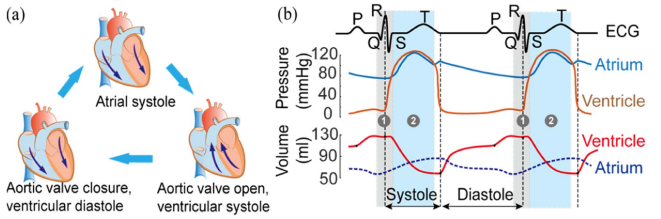

Fig. 16. (a) Cardiac cycle phases. (b) modified wiggers diagram with grey zone indicating 1 (PEP) and blue zone indicating 2 (LEVT). [88].

The STIs represents the duration of total electro-mechanical systole with two commonly used time intervals, i.e., PEP and LVET [86]. The determination of STIs offers an efficient method to study changes in left ventricular performance and the effects of therapeutic interventions or diseases on myocardial performance [86]. PEP and LVET have been known to be useful for the evaluation of cardiac function. Specifically, the PEP/LVET ratio has been shown to be the most sensitive index of ventricular function [87]. In addition, the PEP can be used to improve blood pressure estimation based on pulse arrival time [87], as shown in Fig. 16.

In the context of radar-based measurement of cardiac activity time intervals, the focus lies primarily on the identification and detection of characteristic waveforms associated with certain mechanical activities of the heart. These specific time points may correspond to different states of cardiac activity, giving rise to radar waveforms of varying morphologies. Therefore, in this process, a crucial aspect is the comprehension of the cardiac activity waveforms detected by the radar.

Recent efforts in this domain involve the integration of various medical sensors and measuring instruments, simultaneously with radar devices, to detect cardiac activity in patients within clinical environments [88]. Through this approach, researchers have validated various cardiac activity intervals, such as STI, computed from radar cardiograms. This integrated methodology enhances the understanding of radar-detected cardiac activity waveforms and contributes to a more comprehensive assessment of cardiac function in clinical settings.

Another widely studied cardiac interval that has garnered significant attention from scholars is the measurement of the heart's QRS-QRS interval (RRI). The accurate measurement of the heart's RRI forms the basis for calculating Heart rate variability (HRV). HRV has become a reliable index on assessing humans' mental state and physical condition [89], [90], and has been applied to sleep monitoring [89] and stress recognition [90]. Strictly defined, the RRI is the time interval between QRS complexes in consecutive electrocardiogram waveforms. Currently, radar-based HRV measurement approaches can be classified into two main categories.

One approach involves estimating the heart rate from radar signals within a short time window and then using the variations in heart rate to approximate HRV parameters [91], [92]. The second approach adheres to the medical definition of the RR interval, identifying waveforms in the radar demodulation signals

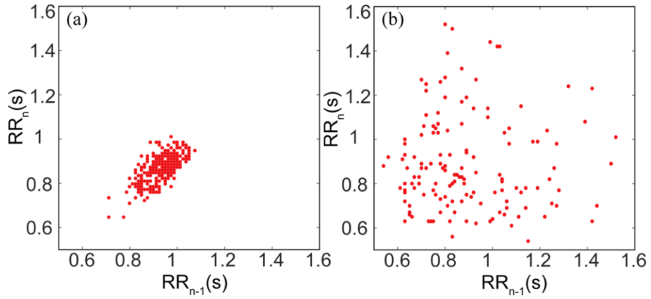

Fig. 17. RR Lorenz plots of radar-based clinical experiments data. (a) Result of normal patient. (b) Result of AF patient. [85].

that correspond to the QRS complexes in the electrocardiogram for precise RRI calculations [93], [94], [95].

D. Radar-Based Cardiovascular Disease Detection

As previously mentioned, with a significant improvement in the accuracy of radar displacement sensing and optimization through preliminary clinical testing, existing biomedical radar systems are now capable of perceiving rich physiological micromotion information in the human body. Particularly noteworthy is the precise detection of cardiac mechanical activity, showcasing the enormous potential of biomedical radar in cardiovascular disease detection.

Atrial fibrillation (AF) is a common cardiac arrhythmia characterized by irregular and often rapid heartbeats. This condition occurs when the upper chambers of the heart, known as the atria, experience chaotic electrical signals, leading to an irregular rhythm [96]. Atrial fibrillation is often associated with other cardiovascular conditions, such as hypertension and heart failure. Detecting early AF symptoms provides an opportunityto assess and manage overall cardiovascular health, addressing contributing factors and minimizing the risk of further complications [97].

In [85], the authors achieved the detection of mechanical cardiogram in patients with persistent atrial fibrillation within a clinical setting. Additionally, they generated a Lorenz plot by extracting RRI parameters, providing a visual representation of the irregularity in cardiac activity during the monitoring time period, as depicted in Fig. 17(b). In comparison to the RR Lorenz plot of normal individuals shown in Fig. 17(a), the RR Lorenz plot of atrial fibrillation patients exhibited a scattered fan-shaped pattern due to the complete arrhythmia in cardiac activity.

Furthermore, certain cardiovascular diseases can induce abnormalities in the mechanical activity of the heart, resulting in disturbances in the waveform of a specific cycle on the cardiogram. For instance, researchers detected patients with occasional premature heartbeats in a clinical setting. At the moments when premature heartbeats occurred, significant deviations in the RR intervals were observed, as depicted in Fig. 18(a). Additionally, substantial waveform disturbances in the D-DCG were evident during these occurrences, as illustrated in Fig. 18(b).

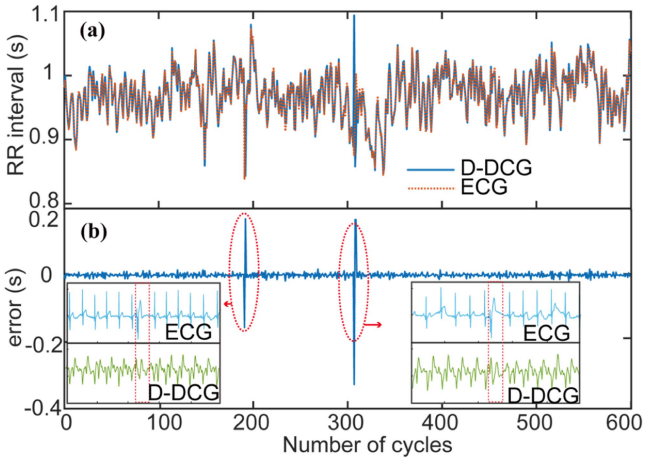

Fig. 18. (a) Comparison between the RRI retrieved from the detected ECG and DCGs for long-term monitoring. (b) The RRI error estimated by D-DCG waveform with respect to ECG. Inserts are detailed ECG and D-DCG waveforms at the cycles when the error suddenly increased. [85].

E. Blood Pressure (BP) Detection

Blood pressure, an indicator of cardiovascular function, is routinely measured in clinical settings. The digital sphygmomanometer with an upper arm cuff has become the most popular device for BP measurement. However, this cuff-style monitor has limitations, for it does not offer real-time continuous BP monitoring, and the process of inflating the cuff can cause discomfort to patients. In home healthcare monitoring, there is a growing trend towards using sleeveless methods that rely on distal pulses, pulse transit time (PTT), and pulse wave velocity (PWV) for continuous BP measurement. These alternative approaches are being explored because they demonstrate a short-term correlation with BP, leading to potential substitutions [98], [99]. In addition to methods based on Photoplethysmography (PPG) [100], accelerometers [101], flexible pressure sensors [102], and ultrasonic phased arrays [103], the use of radar-based approaches for measuring blood pressure is also gaining attention due to their high sensitivity and integrability.

Continuous sleeveless blood pressure monitoring typically involves calculations based on the Moens-Korteweg (MK) equation, Hughes equation, and Bramwell-Hill equation. These equations assume that the artery wall is a thin and fixed shell, with unchanging thickness and radius despite blood pressure variations. Therefore, systolic blood pressure (SBP) and diastolic blood pressure (DBP) can be expressed as

$$DBP = SBP_0 / 3 + 2DBP_0 / 3 + 2ln(PTT_0 / PTT) - (SBP_0 - DBP_0)(PTT_0 / PTT)^2 / 3, \quad (30)$$

$$SBP = DBP + (SBP_0 - DBP_0)(PTT_0 / PTT)^2, \quad (31)$$

where PTT_0, SBP_0, and DBP_0 are the correction values, which can be set as the average values of the training set. PTT can be calculated as the time difference between the heartbeat signal peak and the corresponding feature of the pulse signal

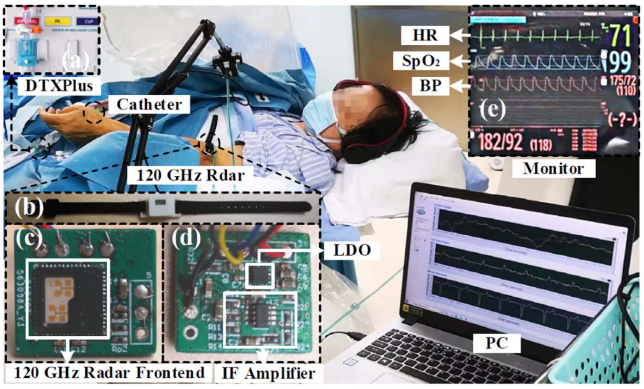

Fig. 19. Experimental setup: (a) the main pressure transducer; (b) outer packing of the 120 GHz radar system; (c) top view of the radar PCB; (d) bottom view of the radar PCB; (e) the simultaneous monitor screenshot. [114].

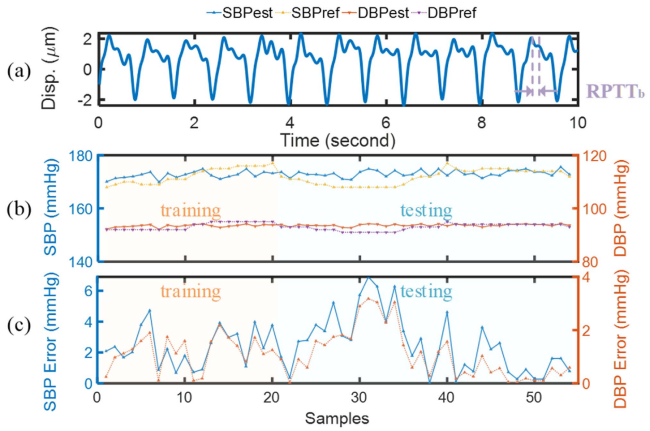

Fig. 20. The estimated and reference blood pressure of a patient. [114].

using two sensors. Alternatively, using only one sensor, PTT can be replaced with RPTT, which is the time interval between two different peaks in one cycle of the pulse signal. This relationship between RPTT and PTT is linear [104], indicating information about artery performance. Certainly, there are multiple alternative models for calculating BP in sleeveless devices, including advanced cardiovascular models, including the Fung hyperelastic model [105] and the incorporation of other factors such as HR [106].

There are several researches of the radar-based continuous BP measurement methods using different principles, such as PTT-based [107], [108], [109], RPTT-bases [110], [111], PWV-based [112], pluse-based [113]. However, most of the studies were carried out on healthy subjects in normal environments. In [114], a noninvasive and continuous blood pressure estimation technique based on a 120 GHz miniaturized radar is proposed. The clinical experimental setup is shown in Fig. 19, in which the invasive pressure transducer was set as reference, and the 120 GHz radar was placed at the patient's elbow. Signals of both sensors were collected for about 2 minutes in every trial when patients were staying calm after surgery. Since each pulse corresponds to a RPTT, SBP, and DBP, the real-time continuous BP estimation can be achieved by acquiring every RPTT of pulse waveforms and converting them to SBP and DBP through a prediction model. The results as displayed in Fig. 20 show that the testing errors are larger than those in the training set, but all of the mean errors of different inpatients are below 3 mmHg in the post-operation experiments, illustrating a great performance of the sensor system in BP prediction in such scenario.

Another clinical research carried out by Heydari F et al. (2020) [115] conducted a clinical study on cuffless BP calculation using PTT measurements. They extracted PTT as the time difference between the end of the pre-ejection period (PEP), measured using an on-body continuous-wave radar sensor or ECG, and the pulse arrival time (PAT) in central arteries derived from bio-impedance signals at the shoulders. The study included 43 volunteers who underwent posture recordings, exercise, and glyceryl trinitrate (GTN) spray. The findings showed that sleeveless BP determined from PTT in central arteries exhibited over 3% higher accuracy compared to peripheral arteries, achieving 93.71% accuracy for SBP and 99.39% accuracy for DBP.

C. Liao et al. (2021) [116] used the Blumio sensor, a fully integrated FMCW system operating in the 57 to 63 GHz band, to detect pulses over the left radial artery on the left wrist. A total of 120 healthy volunteers, aged 20–67 years, were enrolled, and their radar data was processed using Blumio's proprietary waveform transformation and BP estimation algorithm. The results from 70 healthy volunteers demonstrated a mean error of 1.70 mmHg (with a standard deviation of 5.59 mmHg) for SBP and a mean error of 2.85 mmHg (with a standard deviation of 5.57 mmHg) for DBP.

VI. AI-Driven Clinical Applications Based on Radar System

AI-driven clinical applications based on radar systems represent a cutting-edge approach in healthcare technology, offering innovative solutions for various medical scenarios. Radar technology, traditionally associated with remote sensing and navigation, has found novel applications in healthcare, particularly in monitoring and diagnosing physiological conditions.

A. Remote Patient Monitoring

Recently, the aging population has become a significant global concern, leading to an increased focus on developing innovative technologies to support elderly individuals in maintaining independent and healthy lives. One promising avenue is the utilization of radar-based systems for supervising the elderly. These systems offer non-intrusive and continuous monitoring, addressing the need for unobtrusive healthcare solutions.

Matsui et al. (2013) present a practicable, non-contact, autonomic activation monitoring system using microwave radars without imposing any stress on monitored individuals, as shown in Fig. 21. The system allows monitoring of geriatric autonomic dysfunctions caused by chronic diseases, such as diabetes or myocardial infarction (MI), while measuring vital signs in non-contact way. This system measures heart rate variability (HRV) of elderly people in non-contact way using small 24-GHz

Fig. 21. The radar equipment of a non-contact bedside autonomic activation monitoring system. Dual 24-GHz microwave radars are attached beneath the mattress of the patient's bed. [117].

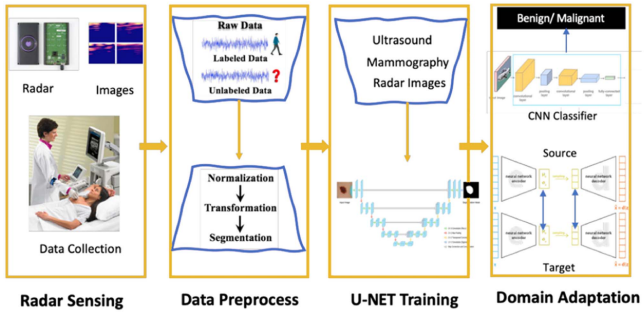

Fig. 22. Overall system architectural diagram of a low-cost radar-based domain adaptive breast cancer screening system. [125].

microwave radars that are attached beneath the mattress of the patient's bed [117]. The measured HRV is widely accepted as an indicator of the autonomic nervous system, which can be also used as a predictor of prognosis of patients with hypertrophic cardiomyopathy [118]. The emphasis on autonomic activation monitoring indicates a shift towards more comprehensive health monitoring systems, capturing physiological responses that may not be evident through traditional monitoring methods.

The study by Diraco et al. (2017) introduces a radar-based smart sensor designed for unobtrusive elderly monitoring in ambient assisted living applications. Based on the proposed ultra-wideband radar, the smart sensor can detect both cardiorespiratory and body movements, which are further used to detect the abnormalities during daily activities such as fall events [119]. Yen et al. (2022) contribute to the literature by developing a medical radar system specifically designed for non-contact vital sign monitoring in hospitalized older patients. The system uses the support-vector machine to evaluate radar signal quality for denoising and uses the singular value decomposition method to extract heartbeat and respiration signals [120]. The emphasis on clinical performance evaluation indicates a step towards the integration of radar-based systems into mainstream healthcare, showcasing the potential impact on the elderly care and management.

B. Microwave Radar Imaging

Breast cancer remains a global health concern, prompting continuous advancements in detection methods to improve early diagnosis and treatment outcomes. Among the innovative approaches, the integration of imaging technologies, breast screening techniques, and respiratory gating of PET/CT has gained significant attention.

In breast microwave radar imaging (BMRI) approaches, the breast is interrogated with ultra-wide-band (UWB) pulses, and backscatter signals are reconstructed into a reflectivity map of the breast where tumors have the strongest response. Klemm et al. contribute to the literature by detailing clinical trials involving a UWB imaging radar for breast cancer. The UWB approach enables high-resolution imaging, potentially improving the accuracy of breast cancer [121]. Porter et al. delve into an early clinical study involving time-domain microwave radar for breast health monitoring. Their radar system operates in the 2–4 GHz range and contains 16 wideband sensors embedded in a hemispherical dielectric redome. Their findings suggest the feasibility of utilizing radar technology for continuous monitoring, providing valuable data for breast health assessment [122]. Solis-Nepote et al. present an air-operated bistatic system for breast microwave radar imaging, demonstrating promising pre-clinical validation results. The system operates in the range of 1–8 GHz and employs a double-ridged horn antenna array with four degrees of freedom. Experiments validate that the system is capable of detecting the presence of a 1.5 cm diameter tumor in a hemispherical breast phantom [123].

While radar imaging technologies aim at creating detailed images or maps of the target area, radar screening focuses on detecting and tracking tumors within a given area. Microwave technologies are suitable for frequent screening because of the non-ionizing radiation and non-invasive nature, and are available at a low cost. Kranold et al. analyze the effect that patient attributes have on the signal strength in a clinical study conducted with a time-domain microwave-radar breast health monitor. The 50 antenna pairs with the highest mean peak amplitude were selected and analyzed for each patient. This literature attributes to optimizing the clinical breast screening prototype and improving the overall signal quality for breast cancer detection. [124]. Claflin et al. propose a low-cost radar-based domain adaptive breast cancer screening system. They developed a deep learning-based domain adaptation model that can learn breast segmentation and cancer detection from expensive source data (mammography, ultrasound) and transfer the knowledge to less expensive target data (Radar data) [125]. The overall architectural diagram of this breast cancer screen system is shown in Fig. 22.

Another innovative breast cancer detection and radiotherapy avenue is the integration of respiratory gating into positron emission tomography/computed tomography (PET/CT) for improved precision. Gu et al. presented a significant contribution to the field by introducing a DC-coupled continuous-wave radar sensor for accurate respiration measurement. The concept of a radiotherapy system with radar sensing has been introduced. As shown in Fig. 23, during radiotherapy, the multiple radars keep tracking the real-time chest wall and abdomen motion and

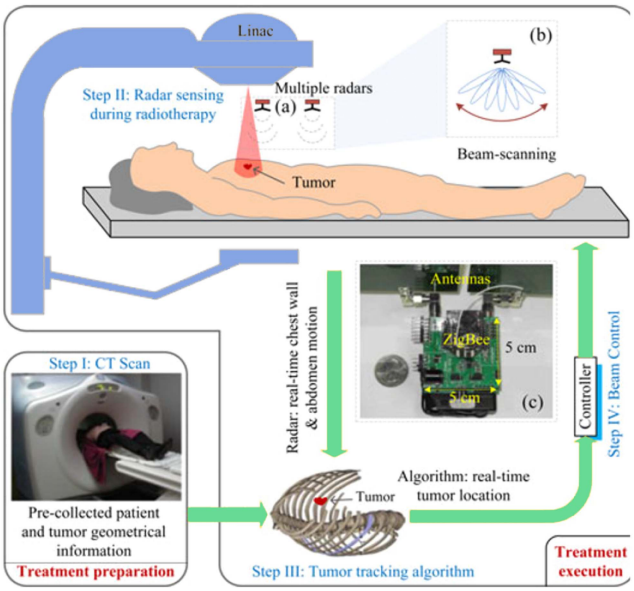

Fig. 23. Motion-adaptive radiotherapy based on radar respiration sensing. The process includes two steps: treatment preparation and treatment execution. Insets: (a) multiple radars, (b) beam-scanning radar, and (c) designed 2.4-GHz miniature radar sensor seating with a quarter [126].

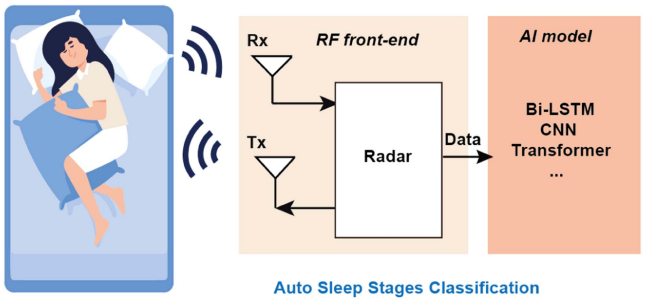

Fig. 24. Radar-based sleep monitoring.

predicting real-time tumor location using the proposed tumor tracking algorithm. Then, a controller utilizes the extracted tumor location information to control the LINAC to either perform gated radiotherapy or steer the radiation beam to track the tumor [126]. Ghahremani et al. introduced a low-power UHF CW Doppler radar system with antennas between the bed and the patient's back to steer the main beam radiation toward the diaphragm. This research highlighted advancements in radar technology, particularly the phased-array configuration, and its potential to further improve the accuracy of respiratory motion measurement. It has demonstrated that radar-based gating of PET/CT can be used to sharpen the PET image [127].

C. Sleeping Monitoring

As shown in Fig. 24, Radar-based sleep monitoring is an innovative and non-intrusive approach to assessing and analyzing sleep patterns and quality. Leveraging radar technology and often enhanced by AI algorithms, this method enables continuous and remote monitoring of an individual's sleep without the need for physical contact or wearable devices.

Hyun Bin Kwon et al. proposed an attention-based bidirectional long short-term memory (Attention Bi-LSTM) model for automatic sleep stage scoring using an impulse-radio ultra-wideband (IR-UWB) radar [128]. Maytus Piriyajitakonkij et al. investigated the performance of an off-the-shelf single antenna UWB in a novel application of sleep postural transition (SPT) recognition. The proposed Multi-View Learning, entitled Sleep-PoseNet or SPN, with time series data augmentation aims to classify four standard SPTs [129].

VII. Conclusion

In conclusion, the recent advancements in biomedical radar technology represent a paradigm shift in clinical applications, offering unprecedented capabilities for non-intrusive and real-time monitoring across a spectrum of healthcare scenarios. From remote patient monitoring to cardiovascular health assessment, respiratory monitoring, and gesture-based surgical control, the versatility of biomedical radar has opened new frontiers in clinical diagnostics and patient care.

The ability of radar systems to provide continuous and detailed physiological insights, coupled with advancements in signal processing and machine learning, positions them as valuable tools in diverse medical domains. Notably, the technology's adaptability in remote patient monitoring, cardiovascular assessment, respiratory health, surgical applications, sleep monitoring, and rehabilitation underscores its potential to revolutionize healthcare practices.

As we look to the future, the continued refinement of radar-based systems, addressing challenges such as improving algorithm accuracy and ensuring privacy in remote monitoring, holds the promise of further expanding the scope of biomedical radar technology. This comprehensive review serves as a testament to the transformative impact of radar systems on clinical applications, emphasizing their potential to enhance diagnostics, optimize patient care, and contribute to the ongoing evolution of healthcare practices. The fusion of radar technology with artificial intelligence is poised to play a pivotal role in shaping the landscape of modern medicine, paving the way for more personalized, efficient, and accessible healthcare solutions.

Conflict of Interest Statement

The authors declare that they have no conflict of interest.

Author Contributions Statement

The authors of this manuscript are Shuqin Dong, Li Wen, Yangtao Ye, Zhi Zhang, Yi Wang, Zhiwei Liu, Cao Qing, Yuchen Xu, Changzhi Li and Changzhan Gu. Shuqin Dong and Li Wen contributed to the whole manuscript writing and revisions. Yangtao Ye contributed to the content of AI-driven medical applications. Dr. Zhi Zhang, Dr. Yi Wang, Dr. Zhiwei Liu, Dr. Cao Qing, Dr. Yuchen Xu provided medical expertise and clinical environment. Prof. Changzhi Li provided valuable insights in

the field of radar systems. Prof. Changzhan Gu contributed to the overall supervision, direction and planning.

REFERENCES

[1] J. C. Lin, "Noninvasive microwave measurement of respiration," *Proc. IEEE*, vol. 63, no. 10, pp. 1530–1530, Oct. 1975.

[2] J. C. Lin, "Microwave sensing of physiological movement and volume change: A review," *Bioelectromagnetics*, vol. 13, pp. 557–565, Dec. 1992.

[3] A. D. Droitcour, O. Boric-Lubecke, V. M. Lubecke, J. Lin, and G. T. A. Kovac, "Range correlation and I/Q performance benefits in single-chip silicon doppler radars for noncontact cardiopulmonary monitoring," *IEEE Trans. Microw. Theory Techn.*, vol. 52, no. 3, pp. 838–848, Mar. 2004.

[4] C. Li, J. Ling, J. Li, and J. Lin, "Accurate Doppler radar noncontact vital sign detection using the RELAX algorithm," *IEEE Trans. Instrum. Meas.*, vol. 59, no. 3, pp. 687–695, Mar. 2010.

[5] Y. Xiong, S. Chen, X. Dong, Z. Peng, and W. Zhang, "Accurate measurement in Doppler radar vital sign detection based on parameterized demodulation," *IEEE Trans. Microw. Theory Techn.*, vol. 65, no. 11, pp. 4483–4492, Nov. 2017.

[6] F.-K. Wang, P.-H. Juan, D.-M. Chian, and C.-K. Wen, "Multiple range and vital sign detection based on single-conversion self-injection-locked hybrid mode radar with a novel frequency estimation algorithm," *IEEE Trans. Microw. Theory Techn.*, vol. 68, no. 5, pp. 1908–1920, May 2020.

[7] M. Li and J. Lin, "Wavelet-transform-based data-length-variation technique for fast heart rate detection using 5.8- GHz CW Doppler radar," *IEEE Trans. Microw. Theory Techn.*, vol. 66, no. 1, pp. 568–576, Jan. 2018.

[8] W. Xia, Y. Li, and S. Dong, "Radar-based high-accuracy cardiac activity sensing," *IEEE Trans. Instrum. Meas.*, vol. 70, 2021, Art. no. 4003213.

[9] S. Dong et al., "Doppler cardiogram: A remote detection of human heart activities," *IEEE Trans. Microw. Theory Techn.*, vol. 68, no. 3, pp. 1132–1141, Mar. 2020.

[10] C. Li, V. M. Lubecke, O. Boric-Lubecke, and J. Lin, "A review on recent advances in Doppler radar sensors for noncontact healthcare monitoring," *IEEE Trans. Microw. Theory Techn.*, vol. 61, no. 5, pp. 2046–2060, May 2013.

[11] D. K. Kim and Y. Kim, "Quadrature frequency-group radar and its center estimation algorithms for small vibrational displacement," *Sci. Rep.*, vol. 9, no. 1, May 2019, Art. no. 6763.

[12] H. Wang, H. Afzal, and O. Momeni, "A highly accurate and sensitive mmWave displacement-sensing doppler radar with a quadrature-less edge-driven phase demodulator," *IEEE J. Solid-State Circuits*, vol. 58, no. 9, pp. 2451–2465, Sep. 2023.

[13] T.-H. Liu, M.-L. Hsu, and Z.-M. Tsai, "High ranging accuracy and wide detection range interferometry based on frequency-sweeping technique with vital sign sensing function," *IEEE Trans. Microw. Theory Techn.*, vol. 66, no. 9, pp. 4242–4251, Sep. 2018.

[14] S. Srinivas, Y. Rong, and D. W. Bliss, "UWB radar cardiac activity sensing: Novel arctangent demodulator for direct-RF receivers," in *Proc. IEEE Int. Radar Conf.*, 2020, pp. 984–989.

[15] J. Wang, X. Wang, L. Chen, J. Huangfu, C. Li, and L. Ran, "Noncontact distance and amplitude-independent vibration measurement based on an extended DACM algorithm," *IEEE Trans. Instrum. Meas.*, vol. 63, no. 1, pp. 145–153, Jan. 2014.

[16] W. Xu, Y. Li, C. Gu, and J.-F. Mao, "Large displacement motion interferometry with modified differentiate and cross-multiply technique," *IEEE Trans. Microw. Theory Techn.*, vol. 69, no. 11, pp. 4879–4890, Nov. 2021.

[17] R. Khanna, D. Oh, and Y. Kim, "Through-wall remote human voice recognition using Doppler radar with transfer learning," *IEEE Sensors J.*, vol. 19, no. 12, pp. 4571–4576, Jun. 2019.

[18] R. Pallas-Areny and O. Casas, "A novel differential synchronous demodulator for AC signals," *IEEE Trans. Instrum. Meas.*, vol. 45, no. 2, pp. 413–416, Apr. 1996.

[19] F. Tong, J. Liu, C. Gu, and J. Mao, "Measurement of displacement motions based on unsynchronized bandpass sampling with a low-IF Doppler radar," in *Proc. IEEE/MTT-S Int. Microw. Symp.*, 2022, pp. 711–714.

[20] G. Wang, J.-M. Muñoz-Ferreras, C. Gu, C. Li, and R. Gómez-García, "Application of linear-frequency-modulated continuous-wave (LFMCW) radars for tracking of vital signs," *IEEE Trans. Microw. Theory Techn.*, vol. 62, no. 6, pp. 1387–1399, Jun. 2014.

[21] J. Schorlemer, C. Schulz, N. Pohl, I. Rolfes, and J. Barowski, "Compensation of sensor movements in short-range FMCW synthetic aperture radar algorithms," *IEEE Trans. Microw. Theory Techn.*, vol. 69, no. 11, pp. 5145–5159, Nov. 2021.

[22] M. Inamori, A. M. Bostamam, Y. Sanada, and H. Minami, "IQ imbalance compensation scheme in the presence of frequency offset and dynamic DC offset for a direct conversion receiver," *IEEE Trans. Wireless Commun.*, vol. 8, no. 5, pp. 2214–2220, May 2009.

[23] B.-K. Park, O. Boric-Lubecke, and V. M. Lubecke, "Arctangent demodulation with DC offset compensation in quadrature doppler radar receiver systems," *IEEE Trans. Microw. Theory Techn.*, vol. 55, no. 5, pp. 1073–1079, May 2007.

[24] G. Wang, J.-M. Muñoz-Ferraras, C. Gu, C. Li, and R. Gómez- García, "Application of linear-frequency-modulated continuouswave (LFMCW) radars for tracking of vital signs," *IEEE Trans. Microw. Theory Techn.*, vol. 62, no. 6, pp. 1387–1399, Jun. 2014.

[25] Z. Peng et al., "A portable FMCW interferometry radar with programmable low-IF architecture for localization, ISAR imaging, and vital sign tracking," *IEEE Trans. Microw. Theory Techn.*, vol. 65, no. 4, pp. 1334–1344, Apr. 2017.

[26] A. Ahmad, J. C. Roh, D. Wang, and A. Dubey, "Vital signs monitoring of multiple people using a FMCW millimeter-wave sensor," in *Proc. IEEE Radar Conf.*, 2018, pp. 1450–1455.

[27] M. Mercuri, I. R. Lorato, Y. Liu, F. Wieringa, C. V. Hoof, and T. Torfs, "Vital-sign monitoring and spatial tracking of multiple people using a contactless radar-based sensor," *Nature Electron.*, vol. 2, pp. 252–262, Jun. 2019.

[28] M. Alizadeh, G. Shaker, and S. Safavi-Naeini, "Experimental study on the phase analysis of FMCW radar for vital signs detection," in *Proc. 13th Eur. Conf. Antennas Propag.*, 2019, pp. 1–4.

[29] M. Alizadeh, G. Shaker, J. C. M. D. Almeida, P. P. Morita, and S. Safavi-Naeini, "Remote monitoring of human vital signs using mm-wave FMCW radar," *IEEE Access*, vol. 7, pp. 54958–54968, 2019.

[30] A. D. Droitcour, O. Boric-Lubecke, V. M. Lubecke, J. Lin, and G. T. A. Kovacs, "Range correlation and I/Q performance benefits in single-chip silicon doppler radars for noncontact cardiopulmonary monitoring," *IEEE Trans. Microw. Theory Techn.*, vol. 52, no. 3, pp. 838–848, Mar. 2004.

[31] K. Ramasubramanian and T. Instruments, "Using a complex-baseband architecture in FMCW radar systems." Texas Instruments, vol. 19, 2017.

[32] J. Liu, Y. Li, C. Li, C. Gu, and J.-F. Mao, "Accurate measurement of human vital signs with linear FMCW radars under proximity stationary clutters," *IEEE Trans. Biomed. Circuits Syst.*, vol. 15, no. 6, pp. 1393–1404, Dec. 2021.

[33] S. Dong et al., "COVID-SENSE: Radar-based remote respiratory disorder detection in clinical environment," in *Proc. IEEE MTT-S Int. Wireless Symp.*, 2023, pp. 1–3.

[34] International Commission on Non-Ionizing Radiation Protection, "Guidelines for limiting exposure to electromagnetic fields (100 kHz to 300 GHz)," *Health Phys.*, vol. 118, no. 5, pp. 483–524, 2020.

[35] T. Kondo et al., "Laser monitoring of chest wall displacement," *Eur. Respir. J.*, vol. 10, no. 8, pp. 1865–1869, 1997.

[36] B. Beyer et al., "In-vivo analysis of sternal angle, sternal and sternocostal kinematics in supine humans during breathing," *J. Biomech.*, vol. 64, pp. 32–40, 2017.

[37] Z. Li, T. Jin, X. Hu, Y. Song, J. Zhang, and Z. Sang, "Remote respiratory and cardiac motion patterns separation with 4d imaging radars," *IEEE J. Biomed. Health Inform.*, vol. 27, no. 6, pp. 2717–2728, Jun. 2023.

[38] H. Zhao et al., "A noncontact breathing disorder recognition system using 2.4-GHz digital-IF doppler radar," *IEEE J. Biomed. Health Inform.*, vol. 23, no. 1, pp. 208–217, Jan. 2019.

[39] M. Mercuri et al., "2-D localization, angular separation and vital signs monitoring using a SISO FMCW radar for smart long-term health monitoring environments," *IEEE Internet Things J.*, vol. 8, no. 14, pp. 11065–11077, Jul. 2021.

[40] S. Gastinger et al., "Estimates of ventilation from measurements of rib cage and abdominal distances: A portable device," *Eur. J. Appl. Physiol.*, vol. 109, no. 6, pp. 1179–1189, 2010.

[41] J. B. West, *Respiratory Physiology: The Essentials*. Baltimore, MD, USA: Williams & Wilkins, 2012.

[42] C. Gu et al., "Accurate respiration measurement using DC-coupled continuous-wave radar sensor for motion-adaptive cancer radiotherapy," *IEEE Trans. Biomed. Eng.*, vol. 59, no. 11, pp. 3117–3123, Nov. 2012.

[43] O. Oldenburg et al., "Sleep-disordered breathing in patients with symptomatic heart failure A contemporary study of prevalence in and characteristics of 700 patients," *Eur. J. Heart Fail*, vol. 9, no. 3, pp. 251–257, 2007.

[44] D. D. Sin et al., "Risk factors for central and obstructive sleep apnea in 450 men and women with congestive heart failure," *Amer. J. Respir. Crit. Care Med.*, vol. 160, no. 4, pp. 1101–1106, 1999.

[45] T. Brack et al., "Daytime cheyne-stokes respiration in ambulatory patients with severe congestive heart failure is associated with increased mortality," *Chest*, vol. 132, no. 5, pp. 1463–1471, 2007.

[46] M. Emdin et al., "Prognostic significance of central apneas throughout a 24-hour period in patients with heart failure," *J. Amer. College Cardiol.*, vol. 70, no. 11, pp. 1351–1364, 2017.

[47] P. A. Lanfranchi et al., "Prognostic value of nocturnal cheyne-stokes respiration in chronic heart failure," *Circulation*, vol. 99, no. 11, pp. 1435–1440, 1999.

[48] S. He, Z. Han, C. Iglesias, V. Mehta, and M. Bolic, "A real-time respiration monitoring and classification system using a depth camera and radars," *Front. Physiol.*, vol. 13, 2022, Art. no. 799621.

[49] C. Yuan, M. B. Khan, X. Yang, F. H. Shah, and Q. H. Abbasi, "Cheyne-stokes respiration perception via machine learning algorithms," *Electronics*, vol. 11, no. 6, 2022, Art. no. 958.

[50] L. Wen et al., "Enhancing heart failure monitoring: Biomedical radar-based detection of cheyne-stokes respiration," in *Proc. IEEE Radio Wireless Symp.*, 2024, pp. 42–45.

[51] R. Farre et al., "Accuracy of thermistors and thermocouples as flow-measuring devices for detecting hypopnoeas," *Eur. Respir. J.*, vol. 11, no. 1, pp. 179–182, 1998.

[52] American Academy of Sleep Medicine, "International classification of sleep disorders—third edition (ICSD-3)," *Amer. Acad. Sleep Med. Resour. Library*, vol. 2, pp. 81–2313, 2014.

[53] G. Scebba, G. Da Poian, and W. Karlen, "Multispectral video fusion for non-contact monitoring of respiratory rate and apnea," *IEEE Trans. Biomed. Eng.*, vol. 68, no. 1, pp. 350–359, Jan. 2021.

[54] H. Zhao et al., "A noncontact breathing disorder recognition system using 2.4-GHz digital-IF doppler radar," *IEEE J. Biomed. Health Inform.*, vol. 23, no. 1, pp. 208–217, Jan. 2019.

[55] H. B. Kwon et al., "Attention-based LSTM for non-contact sleep stage classification using IR-UWB radar," *IEEE J. Biomed. Health Inform.*, vol. 25, no. 10, pp. 3844–3853, Oct. 2021.

[56] D. H. Kelly and D. C. Shannon, "Periodic breathing in infants with near-miss sudden infant death syndrome," *Pediatrics*, vol. 63, no. 3, pp. 355–360, Mar. 1979.

[57] D. H. Kelly et al., "Periodic breathing in siblings of sudden infant death syndrome victims," *Pediatrics*, vol. 66, no. 4, pp. 515–520, Oct. 1980.

[58] M. A. Mohr et al., "Quantification of periodic breathing in premature infants," *Physiol. Meas.*, vol. 36, no. 7, pp. 1415–1427, May 2015.

[59] E. C. Eichenwald et al., "Apnea of prematurity," *Pediatrics*, vol. 137, no. 1, Jan. 2016, Art. no. e20153757.

[60] H.-H. Kuo, N.-H. Peng, T. Kao, and W.-C. Hu, "Using ECG surface electrodes in measurement of respiration rate for preterm infants," in *Proc. IEEE Int. Symp. Bioelectron. Bioinf.*, 2014, pp. 1–4.

[61] A. Janvier et al., "Apnea is associated with neurodevelopmental impairment in very low birth weight infants," *J. Perinatol.*, vol. 24, no. 12, pp. 763–768, Dec. 2004.

[62] G. Beltrão et al., "Contactless radar-based breathing monitoring of premature infants in the neonatal intensive care unit," *Sci. Rep.*, vol. 12, no. 1, pp. 1–5, 2022.

[63] L. Wen et al., "Noncontact infant apnea detection for hypoxia prevention with a K-band biomedical radar," *IEEE Trans. Biomed. Eng.*, vol. 71, no. 3, pp. 1022–1032, Mar. 2024.

[64] F. D. V. Ho et al., "Asthma care for all: Lessons from the Philippines," *Lancet Respir. Med.*, vol. 11, no. 6, pp. 513–514, 2023.

[65] W. Wang et al., "Millimetre-wave radar-based spirometry for the preliminary diagnosis of chronic obstructive pulmonary disease," *IET Radar, Sonar Navigation*, vol. 17, no. 12, pp. 1874–1885, 2023.

[66] S.-T. Tseng et al., "A 65-nm CMOS low-power impulse radar system for human respiratory feature extraction and diagnosis on respiratory diseases," *IEEE Trans. Microw. Theory Techn.*, vol. 64, no. 4, pp. 1029–1041, Apr. 2016.

[67] K. V. Loon et al., "Wireless non-invasive continuous respiratory monitoring with FMCW radar: A clinical validation study," *J. Clin. Monit. Comput.*, vol. 30, no. 6, pp. 797–805, Dec. 2016.

[68] M. Alghatrif and J. Lindsay, "A brief review: History to understand fundamentals of electrocardiography," *J. Community Hosp. Intern. Med. Perspectives*, vol. 2, no. 1, Apr. 2012, Art. no. 14383.

[69] J. T. Ottesen, M. S. Olufsen, and J. K. Larsen, *Appl. Math. Models Hum. Physiol.*, Society for Industrial and Applied Mathematics, 2004.

[70] A. M. Katz, *Physiology of the Heart*, 2nd ed. New York, NY, USA: Raven, 1992.

[71] Z. Xia, M. M. H. Shandhi, Y. Li, O. T. Inan, and Y. Zhang, "The delineation of fiducial points for non-contact radar seismocardiogram signals without concurrent ECG," *IEEE J. Biomed. Health Inform.*, vol. 25, no. 4, pp. 1031–1040, Apr. 2021.

[72] H. Jung, J. Kimball, T. Receveur, E. Agdeppa, and O. T. Inan, "Accurate ballistocardiogram based heart rate estimation using an array of load cells in a hospital bed," *IEEE J. Biomed. Health Inform.*, vol. 25, no. 9, pp. 3373–3383, Sep. 2021.

[73] M. Alghatrif and J. Lindsay, "A brief review: History to understand fundamentals of electrocardiography," *J. Community Hosp. Intern. Med. Perspectives*, vol. 2, no. 1, Apr. 2012, Art. no. 14383.

[74] S. M. D. N. Anavekar et al., "Two-dimensional assessment of right ventricular function: An echocardiographic-MRI correlative study," *Echocardiogr.: J. Cardiovasc. Ultrasound Allied Techn.*, vol. 24, no. 5, pp. 452–456, 2007.

[75] R. P. Paiva et al., "Beat-to-beat systolic time-interval measurement from heart sounds and ECG," *Physiol. Meas.*, vol. 33, no. 2, pp. 177–194, 2012.

[76] G. Cybulski et al., "Stroke volume and systolic time intervals: Beat-to-beat comparison between echocardiography and ambulatory impedance cardiography in supine and tilted positions," *Med. Biol. Eng. Comput.*, vol. 42, no. 5, pp. 707–711, 2004.

[77] O. T. Inan et al., "Ballistocardiography and seismocardiography: A review of recent advances," *IEEE J. Biomed. Health Inform.*, vol. 19, no. 4, pp. 1414–1427, Jul. 2015.

[78] X. Guo et al., "Assessing right ventricular function in patients with pulmonary hypertension based on noninvasive measurements: Correlation between cardiac MRI, ultrasonic cardiogram, multidetector CT and right heart catheterization," *J. Cardiovasc. Magn. Reson.*, vol. 17, no. 1, Feb. 2015, Art. no. 185.

[79] S. E. Luijnenburg et al., "Abnormal right atrial and right ventricular diastolic function relate to impaired clinical condition in patients operated for tetralogy of Fallot," *Int. J. Cardiol.*, vol. 167, no. 3, pp. 833–839, 2013.

[80] J. Zhang, Y. Wu, Y. Chen, and T. Chen, "Health-radio: Towards contactless myocardial infarction detection using radio signals," *IEEE Trans. Mobile Comput.*, vol. 21, no. 2, pp. 585–597, Feb. 2022.

[81] J. Chen, D. Zhang, Z. Wu, F. Zhou, Q. Sun, and Y. Chen, "Contactless electrocardiogram monitoring with millimeter wave radar," *IEEE Trans. Mobile Comput.*, vol. 23, no. 1, pp. 270–285, Jan. 2024, doi: 10.1109/TMC.2022.3214721.

[82] F. Tian et al., "An FFT-based DC offset compensation and I/Q imbalance correction algorithm for bioradar sensors," *IEEE Trans. Microw. Theory Techn.*, vol. 72, no. 3, pp. 1900–1910, Mar. 2024.

[83] U. Ha, S. Assana, and F. Adib, "Contactless seismocardiography via deep learning radars," in *Proc. 26th Annu. Int. Conf. Mobile Comput. Netw.*, 2020, Art. no. 62.

[84] Z. Xia, M. M. H. Shandhi, O. T. Inan, and Y. Zhang, "Non-contact sensing of seismocardiogram signals using microwave Doppler radar," *IEEE Sensors J.*, vol. 18, no. 14, pp. 5956–5964, Jul. 2018.

[85] S. Dong, Y. Li, J. Lu, Z. Zhang, C. Gu, and J. Mao, "Accurate detection of Doppler cardiograms with a parameterized respiratory filter technique using a K-band radar sensor," *IEEE Trans. Microw. Theory Techn.*, vol. 71, no. 1, pp. 71–82, Jan. 2023.

[86] K. Tavakolian, "Systolic time intervals and new measurement methods," *Cardiovasc. Eng. Technol.*, vol. 7, pp. 118–125, 2016.

[87] P. Reant et al., "Systolic time intervals as simple echocardiographic parameters of left ventricular systolic performance: Correlation with ejection fraction and longitudinal two-dimensional strain," *Eur. J. Echocardiogr.*, vol. 11, no. 10, pp. 834–844, 2010.

[88] S. Dong, L. Wen, Z. Zhang, C. Gu, and J. Mao, "Contactless measurement of human systolic time intervals based on doppler cardiograms in clinical environment," *IEEE Microw. Wireless Compon. Lett.*, vol. 32, no. 6, pp. 796–799, Jun. 2022.

[89] I. Gritti et al., "Heart rate variability, standard of measurement, physiological interpretation and clinical use in mountain marathon runners during sleep and after acclimatization at 3480 m," *J. Behav. Brainence*, vol. 3, no. 1, pp. 26–48, 2013.

[90] J. F. Thayer et al., "A meta-analysis of heart rate variability and neuroimagine studies: Implications for heart rate variability as a maker of stress and health," *Neurosci. Biobehavioral Rev.*, vol. 36, no. 2, pp. 747–756, 2011.
[91] J. Park et al., "Polyphase-basis discrete cosine transform for real-time measurement of heart rate with CW doppler radar," *IEEE Trans. Microw. Theory Techn.*, vol. 66, no. 3, pp. 1644–1659, Mar. 2018.
[92] C. Gouveia, D. F. Albuquerque, P. Pinho, and J. Vieira, "Bio-radar cardiac signal model used for HRV assessment and evaluation using adaptive filtering," *IEEE Trans. Instrum. Meas.*, vol. 71, 2022, Art. no. 8503810.
[93] W. Hu, Z. Zhao, Y. Wang, H. Zhang, and F. Lin, "Noncontact accurate measurement of cardiopulmonary activity using a compact quadrature doppler radar sensor," *IEEE Trans. Biomed. Eng.*, vol. 61, no. 3, pp. 725–735, Mar. 2014.
[94] W. Xia, Y. Li, and S. Dong, "Radar-based high-accuracy cardiac activity sensing," *IEEE Trans. Instrum. Meas.*, vol. 70, 2021, Art. no. 4003213, doi: 10.1109/tim.2021.3050827.
[95] S. Dong, Y. Li, J. Lu, Z. Zhang, C. Gu, and J. Mao, "Accurate detection of Doppler cardiograms with a parameterized respiratory filter technique using a K-band radar sensor," *IEEE Trans. Microw. Theory Techn.*, vol. 71, no. 1, pp. 71–82, Jan. 2023.
[96] A. Go, "Prevalence of diagnosed atrial fibrillation in adults: National implications for rhythm management and stroke prevention: The AnTicoagulation and risk factors in atrial fibrillation (ATRIA) study," *Jama*, vol. 285, pp. 2370–2375, 2001.
[97] M. Zoni-Berisso et al., "Epidemiology of atrial fibrillation: European perspective," *Clin. Epidemiol.*, vol. 6, pp. 213–220, 2014.
[98] R. Mukkamala et al., "Toward ubiquitous blood pressure monitoring via pulse transit time: Theory and practice," *IEEE Trans. Biomed. Eng.*, vol. 62, no. 8, pp. 1879–1901, Aug. 2015.
[99] A. Chakraborty, D. Goswami, J. Mukhopadhyay, and S. Chakrabarti, "Measurement of arterial blood pressure through single-site acquisition of photoplethysmograph signal," *IEEE Trans. Instrum. Meas.*, vol. 70, 2021, Art. no. 4000310.
[100] X. Ding et al., "Pulse transit time based continuous cuffless blood pressure estimation: A new extension and a comprehensive evaluation," *Sci. Rep.*, vol. 7, 2017, Art. no. 11554.
[101] A. M. Carek et al., "Seismowatch: Wearable cuffless blood pressure monitoring using pulse transit time," *Proc. ACM Interactive Mobile Wearable Ubiquitous Technol.*, vol. 1, no. 3, pp. 1–16, 2017.
[102] N. Luo et al., "Flexible piezoresistive sensor patch enabling ultralow power cuffless blood pressure measurement," *Adv. Funct. Mater.*, vol. 26, no. 8, pp. 1178–1187, 2016.
[103] M. Lin et al., "A fully integrated wearable ultrasound system to monitor deep tissues in moving subjects," *Nature Biotechnol.*, vol. 42, pp. 448–457, 2024.
[104] A. Qasem and A. Avolio, "Determination of aortic pulse wave velocity from waveform decomposition of the central aortic pressure pulse," *Hypertension*, vol. 51, no. 2, pp. 188–195, 2008.
[105] Y. Ma et al., "Relation between blood pressure and pulse wave velocity for human arteries," *Proc. Nat. Acad. Sci.*, vol. 115, no. 44, pp. 11144–11149, 2018.
[106] R. Wang, W. Jia, Z. H. Mao, R. J. Sclabassi, and M. Sun, "Cuff-free blood pressure estimation using pulse transit time and heart rate," in *Proc 12th. Int. Conf. Signal Process.*, 2014, pp. 115–118.
[107] D. Buxi, J.-M. Redouté, and M. R. Yuce, "Cuffless blood pressure estimation from the carotid pulse arrival time using continuous wave radar," in *Proc. IEEE 37th Annu. Int. Conf. Eng. Med. Biol. Soc.*, 2015, pp. 5704–5707.
[108] M.-C. Tang, C.-M. Liao, F.-K. Wang, and T.-S. Horng, "Noncontact pulse transit time measurement using a single-frequency continuous-wave radar," in *Proc. IEEE/MTT-S Int. Microw. Symp.*, 2018, pp. 1409–1412.
[109] L. Wen, Y. Gao, C. Gu, and J. Mao, "PhysioChair: A dual-frequency radar system for noninvasive and continuous detection of physiological signatures," *IEEE Sensors J.*, vol. 22, no. 8, pp. 8224–8233, Apr. 2022.
[110] H. Zhao, X. Gu, H. Hong, Y. Li, X. Zhu, and C. Li, "Non-contact beat-to-beat blood pressure measurement using continuous wave Doppler radar," in *Proc. IEEE/MTT-S Int. Microw. Symp.*, 2018, pp. 1413–1415.
[111] C.-H. Tseng, T.-J. Tseng, and C.-Z. Wu, "Cuffless blood pressure measurement using a microwave near-field self-injection-locked wrist pulse sensor," *IEEE Trans. Microw. Theory Techn.*, vol. 68, no. 11, pp. 4865–4874, Nov. 2020.
[112] I. Kim and Y. A. Bhagat, "Towards development of a mobile RF doppler sensor for continuous heart rate variability and blood pressure monitoring," in *Proc. IEEE 38th Annu. Int. Conf. Eng. Med. Biol. Soc.*, 2016, pp. 3390–3393.
[113] T. Ohata, K. Ishibashi, and G. Sun, "Non-contact blood pressure measurement scheme using doppler radar," in *Proc. IEEE 41st Annu. Int. Conf. Eng. Med. Biol. Soc.*, 2019, pp. 778–781.
[114] L. Wen, S. Dong, Z. Zhang, C. Gu, and J.-F. Mao, "Noninvasive continuous blood pressure monitoring based on wearable radar sensor with preliminary clinical validation," in *Proc. IEEE Int. Microw. Symp.*, 2022, pp. 707–710.
[115] F. Heydari et al., "Clinical study of a chest-based cuffless blood pressure monitoring system," *Med. Devices Sens.*, vol. 3, no. 5, 2020, Art. no. e10091.
[116] C. Liao, O. Shay, E. Gomes, and N. Bikhchandani, "Noninvasive continuous blood pressure measurement with wearable millimeter wave device," in *Proc. IEEE 17th Int. Conf. Wearable Implantable Body Sensor Netw.*, 2021, pp. 1–5.
[117] T. Matsui et al., "Development of a practicable non-contact bedside autonomic activation monitoring system using microwave radars and its clinical application in elderly people," *J. Clin. Monit. Comput.*, vol. 27, pp. 351–356, 2013.
[118] P. J. Counihan et al., "Assessment of heart rate variability in hypertrophic cardiomyopathy. Association with clinical and prognostic features," *Circulation*, vol. 88, no. 4, pp. 1682–1690, 1993.
[119] G. Diraco, A. Leone, and P. Siciliano, "A radar-based smart sensor for unobtrusive elderly monitoring in ambient assisted living applications," *Biosensors*, vol. 7, no. 4, 2017, Art. no. 55.
[120] H. T. Yen et al., "A medical radar system for non-contact vital sign monitoring and clinical performance evaluation in hospitalized older patients," *Biomed. Signal Process. Control*, vol. 75, 2022, Art. no. 103597.
[121] M. Klemm et al., "Clinical trials of a UWB imaging radar for breast cancer," in *Proc. 4th Eur. Conf. Antennas Propag.*, 2010, pp. 1–4.
[122] E. Porter, M. Coates, and M. Popović, "An early clinical study of time-domain microwave radar for breast health monitoring," *IEEE Trans. Biomed. Eng.*, vol. 63, no. 3, pp. 530–539, Mar. 2016.
[123] M. Solis-Nepote, T. Reimer, and S. Pistorius, "An air-operated bistatic system for breast microwave radar imaging: Pre-clinical validation," in *Proc. IEEE 41st Annu. Int. Conf. Eng. Med. Biol. Soc.*, 2019, pp. 1859–1862.
[124] L. Kranold, C. Quintyne, M. Coates, and M. Popović, "Microwave radar for breast screening: Initial clinical data with suspicious-lesion patients," in *Proc. IEEE 41st Annu. Int. Conf. Eng. Med. Biol. Soc.*, 2019, pp. 3191–3194.
[125] S. Claflin and M. A. Ul Alam, "A low-cost radar-based domain adaptive breast cancer screening system," in *Proc. IEEE MIT Undergraduate Res. Technol. Conf.*, 2020, pp. 1–4.
[126] C. Gu et al., "Accurate respiration measurement using DC-coupled continuous-wave radar sensor for motion-adaptive cancer radiotherapy," *IEEE Trans. Biomed. Eng.*, vol. 59, no. 11, pp. 3117–3123, Nov. 2012.
[127] A. Ghahremani, J. Meier, M. Roknsharifi, J. Hamill, and O. Mawlawi, "Evaluation of phased-array radar-based measurement of respiration during PET/CT," in *Proc. IEEE Nucl. Sci. Symp. Med. Imag. Conf.*, 2018, pp. 1–4.
[128] M. Piriyajitakonkij et al., "SleepPoseNet: Multi-view learning for sleep postural transition recognition using UWB," *IEEE J. Biomed. Health Inform.*, vol. 25, no. 4, pp. 1305–1314, Apr. 2021.
[129] H. B. Kwon et al., "Attention-based LSTM for non-contact sleep stage classification using IR-UWB radar," *IEEE J. Biomed. Health Inform.*, vol. 25, no. 10, pp. 3844–3853, Oct. 2021.